JEM Journal of Experimental Medicine

ARTICLE

ADAM17 is required for EGF-R–induced intestinal tumors via IL-6 trans-signaling

Stefanie Schmidt[1], Neele Schumacher[1], Jeanette Schwarz[1], Simone Tangermann[2], Lukas Kenner[2,3,4], Michaela Schlederer[4], Maria Sibilia[5], Markus Linder[5], Annelore Altendorf-Hofmann[6], Thomas Knösel[7], Elisabeth S. Gruber[8], Georg Oberhuber[4], Julia Bolik[1], Ateequr Rehman[9], Anupam Sinha[9], Juliane Lokau[1], Philipp Arnold[10], Anne-Sophie Cabron[1], Friederike Zunke[1], Christoph Becker-Pauly[1], Adele Preaudet[11,12], Paul Nguyen[11,12], Jennifer Huynh[13], Shoukat Afshar-Sterle[13], Ashwini L. Chand[13], Jürgen Westermann[14], Peter J. Dempsey[15], Christoph Garbers[1], Dirk Schmidt-Arras[1], Philip Rosenstiel[9], Tracy Putoczki[11,12], Matthias Ernst[13], and Stefan Rose-John[1]

Colorectal cancer is treated with antibodies blocking epidermal growth factor receptor (EGF-R), but therapeutic success is limited. EGF-R is stimulated by soluble ligands, which are derived from transmembrane precursors by ADAM17-mediated proteolytic cleavage. In mouse intestinal cancer models in the absence of ADAM17, tumorigenesis was almost completely inhibited, and the few remaining tumors were of low-grade dysplasia. RNA sequencing analysis demonstrated down-regulation of STAT3 and Wnt pathway components. Because EGF-R on myeloid cells, but not on intestinal epithelial cells, is required for intestinal cancer and because IL-6 is induced via EGF-R stimulation, we analyzed the role of IL-6 signaling. Tumor formation was equally impaired in IL-6$^{-/-}$ mice and sgp130Fc transgenic mice, in which only trans-signaling via soluble IL-6R is abrogated. ADAM17 is needed for EGF-R–mediated induction of IL-6 synthesis, which via IL-6 trans-signaling induces β-catenin–dependent tumorigenesis. Our data reveal the possibility of a novel strategy for treatment of colorectal cancer that could circumvent intrinsic and acquired resistance to EGF-R blockade.

Introduction

Colorectal cancer (CRC) is the third most common malignancy in the United States, with ∼50,000 deaths each year (Siegel et al., 2016). Chronic intestinal inflammation (Terzic et al., 2010) and elevated activity of epidermal growth factor receptor (EGF-R) have been associated with increased risk of CRC (Sibilia et al., 2007). CRCs arise after the loss of tumor suppressor genes, including adenomatous polyposis coli (APC), from intestinal epithelial stem cells that reside at the base of the crypt. This is followed by a stepwise accumulation of mutations in oncogenes, such as the Kirsten rat sarcoma virus oncogene *KRAS* (Kinzler and Vogelstein, 1996). The standard of care for unresectable metastatic CRC includes chemotherapy combined with neutralizing antibodies targeting vascular endothelial growth factor (VEGF) or EGF-R (Tobin et al., 2015). Because overexpression of EGF-R is found in the majority of CRC patients, therapeutic inhibition of this signaling cascade is a seemingly obvious treatment option (Haraldsdottir and Bekaii-Saab, 2013). However, it is now clear that EGF-R–blocking antibodies, including cetuximab or panitumumab, are beneficial only in patients who do not harbor *KRAS* mutations (Linardou et al., 2008; Tobin et al., 2015). Unfortunately, even in *KRAS* WT patients with an initial response, resistance against EGF-R blockade almost invariably occurs (Pietrantonio et al., 2017). Therefore, new therapeutic strategies for the treatment of CRC are warranted.

The receptor tyrosine kinase EGF-R controls proliferation, differentiation, gastric barrier function, and cellular survival, highlighting a driving role in various epithelial cancers (Egger et al., 2000; Sibilia et al., 2007). EGF-R belongs to a family of

[1]Biochemisches Institut, Christian Albrechts Universität Kiel, Kiel, Germany; [2]Unit of Laboratory Animal Pathology, University of Veterinary Medicine, Vienna, Austria; [3]Ludwig Boltzmann Institute for Cancer Research, Vienna, Austria; [4]Department of Experimental and Laboratory Animal Pathology, Medical University Vienna, Vienna, Austria; [5]Institute of Cancer Research, Department of Medicine I, Medical University of Vienna, Comprehensive Cancer Center, Vienna, Austria; [6]Department of General, Visceral and Vascular Surgery, Jena University Hospital, Jena, Germany; [7]Institute of Pathology, Ludwig-Maximilians-University, Munich, Germany; [8]Department of General Surgery, Division of Surgery and Comprehensive Cancer Center, Medical University Vienna, Vienna, Austria; [9]Institute of Clinical Molecular Biology, Christian Albrechts Universität Kiel, Kiel, Germany; [10]Anatomisches Institut, Christian Albrechts Universität Kiel, Kiel, Germany; [11]The Walter and Eliza Hall Institute of Medical Research, Melbourne, VIC, Australia; [12]Department of Medical Biology, The University of Melbourne, Melbourne, VIC, Australia; [13]Olivia Newton-John Cancer Research Institute and La Trobe University School of Cancer Medicine, Heidelberg, VIC, Australia; [14]Institut für Anatomie, Universität zu Lübeck, Lübeck, Germany; [15]Department of Pediatrics, University of Colorado School of Medicine, Aurora, CO.

Correspondence to Stefan Rose-John: rosejohn@biochem.uni-kiel.de.

© 2018 Crown copyright. The government of Australia, Canada, or the UK ("the Crown") owns the copyright interests of authors who are government employees. The Crown Copyright is not transferable. This article is distributed under the terms of an Attribution–Noncommercial–Share Alike–No Mirror Sites license for the first six months after the publication date (see http://www.rupress.org/terms/). After six months it is available under a Creative Commons License (Attribution–Noncommercial–Share Alike 4.0 International license, as described at https://creativecommons.org/licenses/by-nc-sa/4.0/).

four receptors (Avraham and Yarden, 2011), which are engaged by 11 different ligands, leading to activation of several signaling pathways often involved in cell fate decisions (Avraham and Yarden, 2011). Each of the ligands for EGF-R is synthesized as a transmembrane precursor protein, which needs to be cleaved to act systemically (Blobel, 2005). This cleavage is performed by members of the ADAM (a disintegrin and metalloprotease) family, with most ligands cleaved by the protease ADAM17, which is a membrane-bound metalloprotease (Black et al., 1997; Moss et al., 1997). To date, more than 80 different substrates have been reported for ADAM17, including TNFα, IL-6 receptor (IL-6R), L-selectin, and both TNFα receptors (Scheller et al., 2011a). As such, ADAM17 regulates the IL-6 trans-signaling pathway through generation of the soluble IL-6R (sIL-6R; Yan et al., 2016), which drives most of the proinflammatory activities of the cytokine IL-6 (Rose-John et al., 2017).

Systemic ADAM17 knockout mice are not viable (Peschon et al., 1998). For this reason, we previously generated hypomorphic ADAM17 mice by inserting an additional exon into the *ADAM17* gene (Chalaris et al., 2010). The new exon starts with an in-frame stop codon that is flanked by splice donor/acceptor sites, which slightly deviate from the canonical consensus sequence. This novel strategy resulted in viable mice, called ADAM17$^{ex/ex}$ mice, with significantly reduced ADAM17 protein levels and no detectable cleaving activity (Chalaris et al., 2010). ADAM17$^{ex/ex}$ mice have eye, hair, and skin defects resembling those in TGFα$^{-/-}$ mice (Chalaris et al., 2010). Interestingly, in ADAM17$^{ex/ex}$ mice, milk duct formation in the female breast, which is known to be EGF-R dependent (Sternlicht et al., 2005), was severely compromised (Chalaris et al., 2010). Furthermore, upon challenge with dextran sodium sulfate (DSS), ADAM17$^{ex/ex}$ mice exhibited defective regeneration of the colonic epithelium, which could be overcome by administration of recombinant EGF-R ligands (Chalaris et al., 2010). From these observations, we hypothesized that in ADAM17$^{ex/ex}$ mice, EGF-R activity was largely abrogated by a lack of EGF-R ligand shedding (Chalaris et al., 2010).

IL-6 is an inflammatory cytokine that plays an important role in inflammatory bowel disease (Atreya et al., 2000) and intestinal cancer (Grivennikov et al., 2009). On target cells, IL-6 binds to the IL-6 receptor (IL-6R), and the complex of IL-6 and IL-6R binds to the ubiquitously expressed signaling receptor subunit gp130, which upon dimerization initiates intracellular signaling via the STAT3 and ERK pathways (Scheller et al., 2011b). Cells that do not express IL-6R cannot respond to IL-6 but can be stimulated by IL-6 bound to a soluble form of the IL-6R (sIL-6R). This signaling pathway, termed IL-6 trans-signaling (Rose-John and Heinrich, 1994), is essential for colitis (Atreya et al., 2000) and other inflammatory diseases (Jones et al., 2011).

In the present study, we analyzed the role of ADAM17 in the development of colon cancer using the *APC*$^{Min/+}$ model of familial adenomatous polyposis, where a heterozygous germ line truncation in the *apc* gene results in the development of small and large intestinal tumors after the spontaneous loss of heterozygosity of the remaining *apc* WT allele (Yamada and Mori, 2007). We found that in the absence of ADAM17, not only was tumor formation abrogated, but also the few residual tumors detected in ADAM17$^{ex/ex}$ mice were of low-grade dysplasia. Furthermore, we could demonstrate that tumor formation required sIL-6R–dependent IL-6 trans-signaling, since it could be inhibited with the IL-6 trans-signaling inhibitory protein sgp130Fc (Jostock et al., 2001). These results suggest that blockade of IL-6 trans-signaling may be a novel CRC therapeutic strategy that could circumvent intrinsic and acquired resistance to EGF-R blockade.

Results

Expression of EGF-R, but not ADAM17, is a prognostic factor for metastatic CRC

Because EGF-R activation requires ADAM17 activity, we analyzed 361 (for ADAM17) and 330 (for EGF-R) human tissue microarray samples from patients with Union for International Cancer Control (UICC) stage II–III surgically resected CRC for EGF-R and ADAM17 expression. In Fig. S1 A, we show representative examples for both proteins expressed at various levels. Fig. S1 (B and C) depicts the highly variable distribution of EGF-R and ADAM17 expression. As reported, overall survival was significantly higher in patients with no, low, and intermediate EGF-R expression compared with patients with high EGF-R expression (Fig. S1 D). However, no significant correlation between ADAM17 expression or ADAM17-positive stained cells and overall survival was detected (Fig. S1 E). This was not completely unexpected, since ADAM17 mRNA is found in virtually all cells (Scheller et al., 2011a; Thul et al., 2017) and regulation of ADAM17 activity occurs mainly at the posttranslational level (Li et al., 2015; Sommer et al., 2016; Grieve et al., 2017). Our data confirm recent studies that EGF-R expression is a prognostic marker for CRC (Hardbower et al., 2017; Srivatsa et al., 2017) with no similar prognostic value for expression of the protease ADAM17. Therefore, we turned our attention to the analysis of the biological activity of EGF-R and ADAM17.

EGF-R activation in human colon cancer cells depends on ADAM17 activity

We found that all seven tested human epithelial colon adenocarcinoma cell lines expressed ADAM17 and EGF-R protein (not depicted). In HCA-7 cells, we detected only EGF-R mRNA, but no expression of other ErbB receptors (Fig. 1 A), highlighting that EGF-R is the dominant ErbB family member present. In addition, HCA-7 cells expressed the EGF-R ligands betacellulin, EGF, amphiregulin, and epiregulin but not the Erb3/4 ligand neuregulin 2 (Fig. 1 A). Interestingly, we found that EGF-R was strongly autophosphorylated in HCA-7 colon adenocarcinoma cells (Fig. 1 B) without exogenous stimulation. This was dependent on the activity of ADAM17 because the inhibition of the ADAM family member ADAM10 with GI254023 (Hundhausen et al., 2003) did not reduce EGF-R phosphorylation, whereas treatment with GW280264, which blocks both ADAM10 and ADAM17 activity (Hundhausen et al., 2003) strongly reduced EGF-R phosphorylation to the same extent as the pan-metalloprotease inhibitor marimastat or the EGF-R kinase inhibitor AG1478 (Zhou and Brattain, 2005). As a control, stimulation of HCA-7 cells with EGF led to a further increase of EGF-R phosphorylation (Fig. 1 B).

Under basal conditions, we detected high levels of soluble amphiregulin in the supernatant of HCA-7 cells, which was not reduced upon ADAM10 inhibition but was drastically reduced

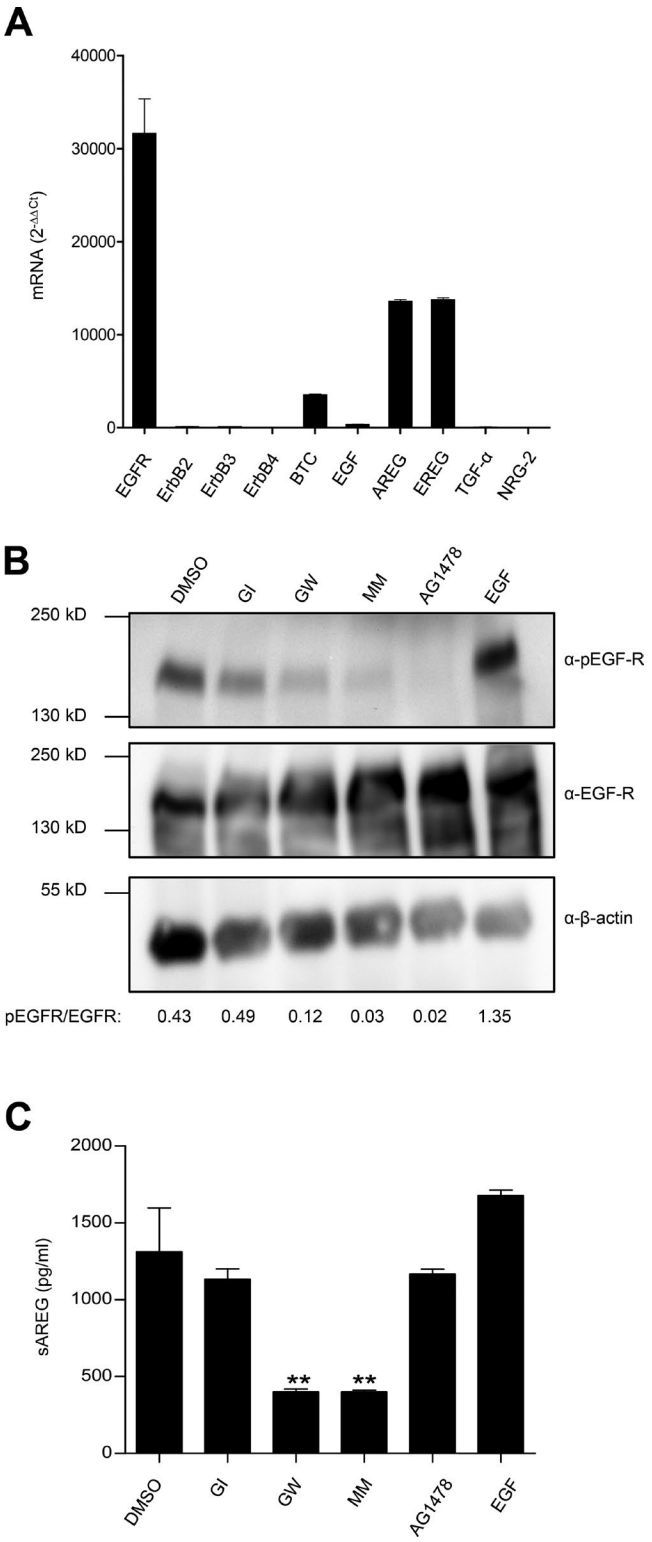

Figure 1. **EGF-R activation in CRC cells depends on ADAM17 activity. (A)** qRT-PCR analysis of members of the EGF-R family and ligands in HCA-7 cells. Two independent experiments were performed and measured in triplicate. Error bars indicate means ± SD. **(B)** Autophosphorylation of EGF-R was inhibited by ADAM17 blockade. HCA-7 cells were treated for 24 h with 0.1% DMSO, the metalloprotease inhibitors GI (GI254023X, ADAM10-selective, 3 µM) and GW (GW280264X, ADAM10- and ADAM17-selective, 3 µM), the pan-metalloprotease inhibitor Marimastat (MM; 10 µM), and the EGF-R kinase inhibitor AG1478 (10 µM). Cells stimulated with 100 ng/ml EGF served as positive control. Tyrosine-phosphorylated EGF-R and total EGF-R were assessed by Western blot analysis. The ratio of intensities of the pEGF-R and EGF-R bands is shown below the blot. One representative of four independent experiments is shown. **(C)** Amphiregulin in cellular supernatants was measured by ELISA. Cells were treated for 24 h with 0.1% DMSO, 3 µM GI254023X, 3 µM GW280264X, 10 µM Marimastat, 10 µM AG1478, or 100 ng/ml human EGF. Three independent experiments were performed, and measurements were done in triplicate. Error bars indicate means ± SD. **, P = 0.0078 (GW) and P = 0.0027 (MM) by unpaired *t* test.

when ADAM17 was inhibited or a broad-spectrum metalloprotease inhibitor was applied. Inhibition of the kinase domain of EGF-R with AG1478 had no influence on soluble amphiregulin levels, whereas EGF stimulation led to a slight increase of this EGF-R ligand in the supernatant (Fig. 1 C). We conclude from these experiments that ADAM17 activity is needed for constitutive EGF-R activation in these colon adenocarcinoma cells, and that this was most likely caused by ADAM17-mediated shedding of EGF-R ligands such as amphiregulin in a process that has been termed trans-activation (Prenzel et al., 1999).

Size of small-intestine organoids from Apc$^{Min/+}$ mice is altered by the absence of ADAM17

Having shown that ADAM17 activity was a prerequisite of EGF-R activation in HCA-7 human colon adenocarcinoma cells, we decided to study Apc$^{Min/+}$ mice, which have only one functional allele of the tumor suppressor Apc. Loss of the remaining Apc WT allele leads to ligand-independent activation of the canonical Wnt signaling cascade, nuclear accumulation of β-catenin, and development of intestinal adenomas primarily in the small intestine (Kimelman and Xu, 2006). ADAM17 protein expression was virtually undetectable in organoids derived from Apc$^{Min/+}$::ADAM17$^{ex/ex}$ compound mutant mice (Fig. S2 A). Single organoids from Apc$^{Min/+}$ and Apc$^{Min/+}$::ADAM17$^{ex/ex}$ mice were similar in spheroid shape (Fig. 2 A, left). As shown in Fig. 2 A (right), in the absence of ADAM17, expression of the proliferation marker Ki67 and the transcription factor T (brachyury), a metastatic tumor marker in colon cancer (Kilic et al., 2011), was decreased. Because organoids were cultured in the presence of EGF but in the absence of IL-6, there was no difference in detectable phosphorylated EGF-R (pEGF-R) and phosphorylated STAT3. However, there were fewer and smaller organoids from Apc$^{Min/+}$::ADAM17$^{ex/ex}$ mice compared with Apc$^{Min/+}$ mice (Fig. 2 B). Expression of the Wnt target genes *c-Myc*, *Axin-2*, *Birc5*, and *Ctgf* was elevated in organoids of Apc$^{Min/+}$ mice compared with WT mice, which was partially rescued in organoids from Apc$^{Min/+}$::ADAM17$^{ex/ex}$ mice, except for *Axin-2*, which showed a similar expression as in organoids derived from Apc$^{Min/+}$ mice (Fig. 2 C). Expectedly, no *IL-6* mRNA was detected in the organoids, whereas expression of *Il-6r* mRNA was up-regulated in organoids with an Apc$^{Min/+}$ background (Fig. S2 B). The mRNA of *Il6st* (gp130) in organoids from Apc$^{Min/+}$ mice was up-regulated in the absence of ADAM17 (Fig. S2 B). We also found high expression of *Yap-1*, *Lats1*, and *Cyr61* in organoids from Apc$^{Min/+}$ mice, which was not changed in the absence of ADAM17

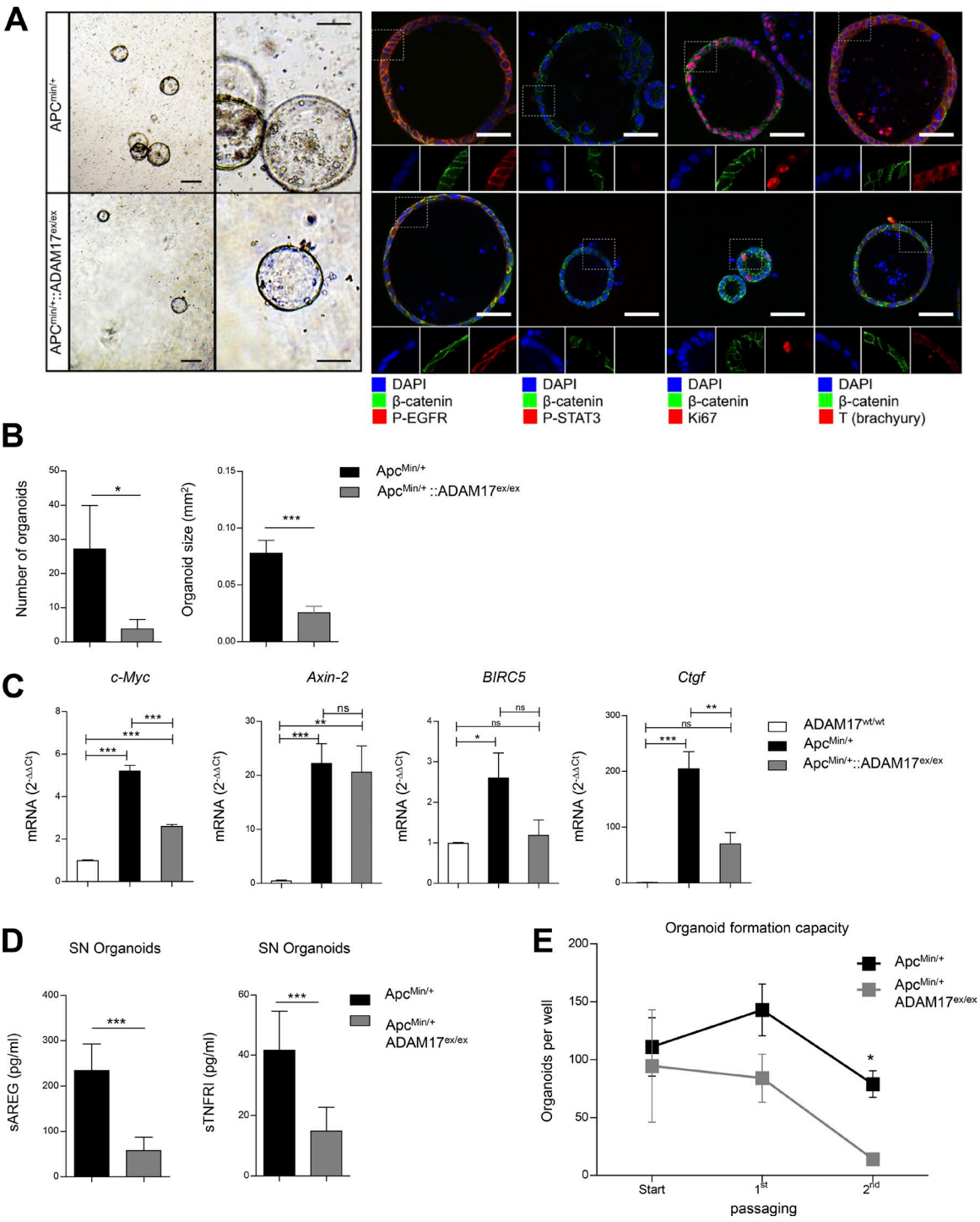

Figure 2. **Effects of ADAM17 on intestinal organoids from Apc$^{Min/+}$ animals. (A)** Left: Bright-field images of APC$^{min/+}$ and APC$^{min/+}$::ADAM17$^{ex/ex}$ intestinal organoids grown in Matrigel spots. Bars, 200 µm in both magnifications. Right: Immunofluorescent staining of intestinal organoids using the primary antibodies indicated in the figure. Top: Merged picture of all three fluorescent channels. Bottom: Magnified areas of the single fluorescent channel, marked by dotted lines in the upper panel. Bars, 50 µm. Three to six high-power-field images were recorded, and representative images are shown. **(B)** Numbers and sizes of primary organoids from Apc$^{Min/+}$::ADAM17$^{ex/ex}$ mice formed 10 d after isolation. Primary organoids were isolated from the small intestine of 24-wk-old Apc$^{Min/+}$ (n = 6) and Apc$^{Min/+}$::ADAM17$^{ex/ex}$ (n = 9) mice. *, P < 0.05; ***, P < 0.001 by Mann–Whitney test. **(C)** qRT PCR analysis of selected target genes from Apc$^{Min/+}$ and Apc$^{Min/+}$::ADAM17$^{ex/ex}$ organoids. Four independent experiments were performed. qRT-PCR was done in triplicate. *, P < 0.05; **, P < 0.01; ***, P < 0.001; ns, nonsignificant by unpaired t test with Welch's correction. **(D)** Levels of soluble proteins in the supernatant of Apc$^{Min/+}$ organoid cultures determined by ELISA. Five independent experiments were performed. ***, P < 0.001 by Mann–Whitney test. **(E)** Plating efficiency of Apc$^{Min/+}$ organoids was reduced in the absence of ADAM17 activity in medium without EGF. Five independent experiments were performed. *, P < 0.05 by two-way ANOVA with Bonferroni post hoc test. Error bars indicate means ± SD.

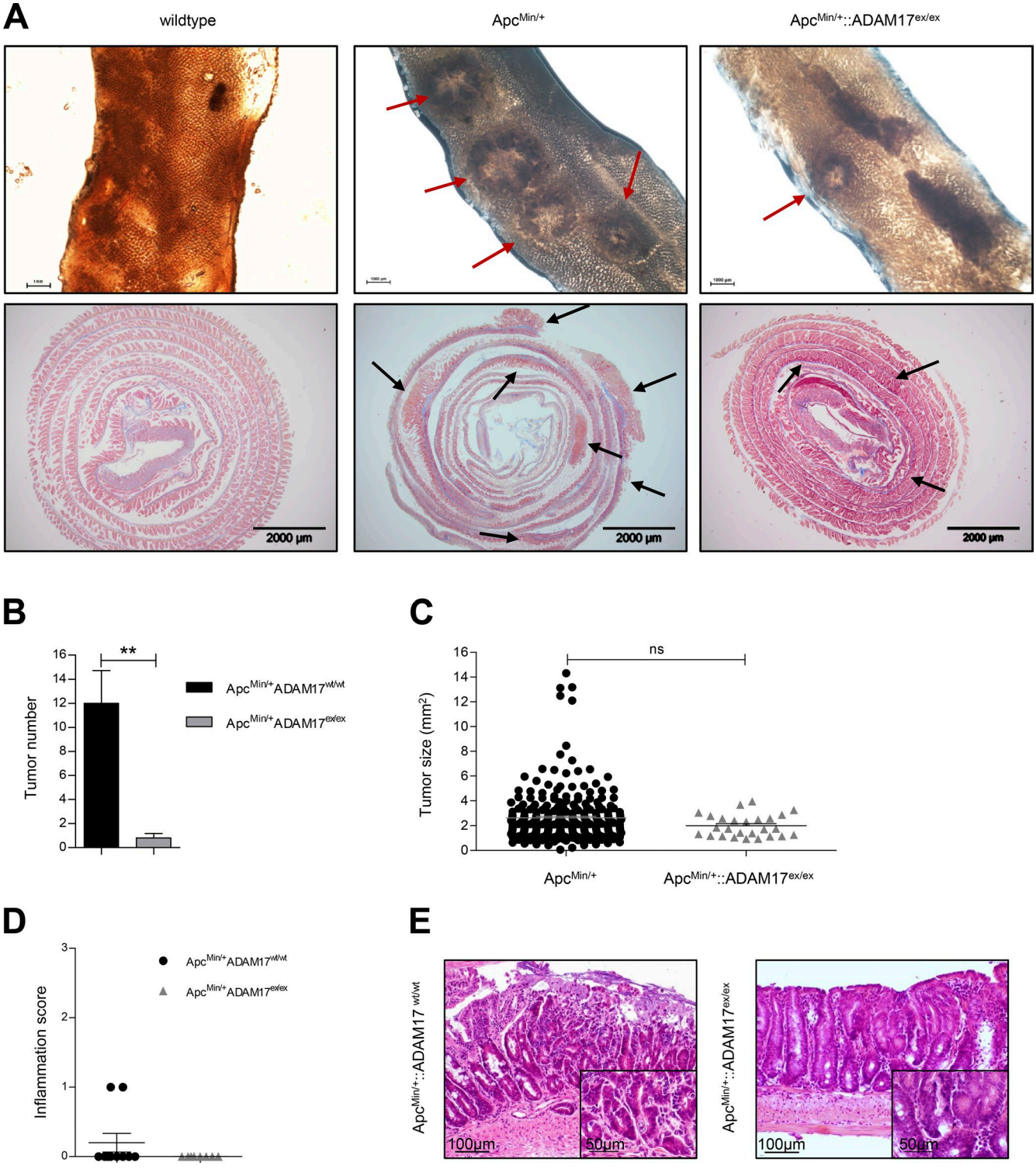

Figure 3. **ADAM17 deficiency reduces intestinal tumor burden. (A)** Representative images of small intestine tissue from WT, $Apc^{Min/+}$, and $Apc^{Min/+}$::$ADAM17^{ex/ex}$ mice. Bars: (top) 1,000 µm; (bottom) 2,000 µm. Arrows point to neoplasias analyzed. **(B and C)** Tumor numbers (B) and tumor sizes (C) were determined macroscopically in the small intestine. $Apc^{Min/+}$ (n = 15) and $Apc^{Min/+}$::$ADAM17^{ex/ex}$ (n = 14) mice were analyzed at 6 mo. **, P < 0.01 by Mann–Whitney test. **(D)** Grading of inflammatory infiltrate in dysplasia from $Apc^{Min/+}$ mice and hypomorphic $Apc^{Min/+}$::$ADAM17^{ex/ex}$ mice. Inflammatory scoring (0, no infiltrate; 1, mild infiltrate; 2, moderate infiltrate; 3, severe infiltrate). $Apc^{Min/+}$ (n = 10) and $Apc^{Min/+}$::$ADAM17^{ex/ex}$ (n = 8) mice. ns, nonsignificant by unpaired t test. **(E)** Representative H&E images of small intestines of $Apc^{Min/+}$ and $Apc^{Min/+}$::$ADAM17^{ex/ex}$ mice. Bars: (panels) 100 µm; (insets) 50 µm. Error bars indicate means ± SD.

(Fig. S2 B). In addition, we showed that shedding of amphiregulin and $TNFR_I$ was strongly reduced in organoids from $Apc^{Min/+}$::$ADAM17^{ex/ex}$ mice (Fig. 2 D), and shedding was further inhibited by the ADAM17 inhibitor GW280264 (Fig. S2 C). Organoids from $Apc^{Min/+}$ and $Apc^{Min/+}$::$ADAM17^{ex/ex}$ mice grew in the absence of the Wnt signaling enhancer R-Spondin-1 and Wnt3a

(not depicted). However, when cultured for two passages in the absence of EGF, organoid cultures from $Apc^{Min/+}$::$ADAM17^{ex/ex}$ mice yielded significantly fewer organoids than cultures from ADAM17-proficient $Apc^{Min/+}$ mice, possibly reflecting the reduced shedding of mature amphiregulin into the culture medium and associated autocrine signaling in the absence of ADAM17 (Fig. 2 E). These results not only confirm that the Wnt pathway is activated in $Apc^{Min/+}$ mice but also that in the absence of ADAM17, Wnt signaling was reduced alongside the capacity to form organoids.

Tumor formation in the $Apc^{Min/+}$ model is reduced in the absence of ADAM17

Although the intestinal architecture and cellularity of $ADAM17^{ex/ex}$ mice was normal (not depicted), these mice were highly susceptible to DSS-induced colitis, suggesting changes to epithelial cell behavior (Chalaris et al., 2010). With this in mind, we next determined the impact of ADAM17 loss on tumorigenesis in the $Apc^{Min/+}$ model, which has previously been shown to be dependent on EGF-R activity (Roberts et al., 2002). We therefore analyzed tumor formation in $Apc^{Min/+}$ and $Apc^{Min/+}$::$ADAM17^{ex/ex}$ mice. Here, lack of ADAM17 resulted in almost complete abrogation of tumorigenesis compared with the high tumor load in the intestine of $Apc^{Min/+}$ mice (Fig. 3, A and B). Interestingly, the few tumors that still occurred in $Apc^{Min/+}$::$ADAM17^{ex/ex}$ mice were of similar size as the tumors found in $Apc^{Min/+}$ mice (Fig. 3 C), indicating that the ADAM17-EGF-R axis plays an important role in the tumor-initiating stage rather than in the outgrowth of the tumors. In $Apc^{Min/+}$ mice, tumors primarily arose in the jejunum and ileum (Fig. S3). Although there was no major increase in the inflammatory infiltrate in dysplasias of both mouse strains (Fig. 3, D and E), in both $Apc^{Min/+}$ and $Apc^{Min/+}$::$ADAM17^{ex/ex}$ mice, we noted increased infiltration of F4/80-positive macrophages in unaffected tissues versus in dysplasias (Fig. S4 A). There was no significant difference in the infiltration of CD3-positive T cells between $Apc^{Min/+}$ and $Apc^{Min/+}$::$ADAM17^{ex/ex}$ mice (Fig. S4 B).

Representative H&E-stained tissue from $Apc^{Min/+}$ and $Apc^{Min/+}$::$ADAM17^{ex/ex}$ mice (Fig. 4 A) indicated that $Apc^{Min/+}$ mice developed low-grade dysplasias, high-grade dysplasias, and carcinomas, as has been described previously (McCart et al., 2008). In contrast, in $Apc^{Min/+}$::$ADAM17^{ex/ex}$ mice, only low-grade dysplasias were detected (Fig. 4, A and B), indicating that in the absence of ADAM17, tumors do not progress beyond this stage. The rather benign status of dysplasia in $Apc^{Min/+}$::$ADAM17^{ex/ex}$ mice is underlined by strongly reduced nuclear β-catenin staining (Fig. 5 A), reduced proliferation as assessed by Ki67 staining (Fig. 5 B), and strongly reduced nuclear STAT3 staining (Fig. 5 C), reflecting reduced STAT3 activation in the absence of ADAM17. These data underline the important role of ADAM17 in not only tumor initiation but also the grade of dysplasia and invasive behavior of tumors.

Our data suggested that ADAM17-mediated shedding of EGF-R ligands is needed for EGF-R activation in tumor development. Recently, it was shown in an inflammation-associated cancer model (Hardbower et al., 2017; Srivatsa et al., 2017), as well as in the $Apc^{Min/+}$ model (Srivatsa et al., 2017), that genetic deletion of the *egfr* gene in intestinal epithelial cells did not result in reduced tumorigenesis, whereas *egfr* deletion in myeloid cells led to a drastic reduction in tumor numbers. It was further shown that EGF-R activation on tumor-infiltrating macrophages led to the secretion of IL-6, which stimulated tumor growth on intestinal epithelial cells (Srivatsa et al., 2017). In line with these findings, we failed to detect significant differences in EGF-R phosphorylation in intestinal sections of $Apc^{Min/+}$ and $Apc^{Min/+}$::$ADAM17^{ex/ex}$ mice (not depicted). We therefore sought to analyze gene expression patterns in tissues and tumors of $Apc^{Min/+}$ mice in the absence or presence of ADAM17 activity to understand the signaling pathways involved in colon cancer formation.

Gene expression analysis of dysplasia from $Apc^{Min/+}$ mice in the presence and absence of ADAM17

To further delineate the molecular mechanism underpinning the effect of ADAM17 on tumor formation, we obtained epithelial mucosa from both tumor and nontumor compartments of $Apc^{Min/+}$ and $Apc^{Min/+}$::$ADAM17^{ex/ex}$ mice by laser capture microdissection. In comparison to healthy tissue from WT animals, tumors from $Apc^{Min/+}$ mice showed high expression of EGF-R and amphiregulin, which was reduced in the absence of ADAM17 (Fig. 6 A). Similar to the situation in organoids (Fig. 2), we also found elevated expression of Wnt target genes and up-regulation of *Il-6*, *Il-6r*, and *birc5* mRNA in tumors from $Apc^{Min/+}$ mice, which were mostly down-regulated in the absence of ADAM17 (Fig. 6 B). Given that IL-6 via STAT3 activation plays a pivotal role in intestinal tumorigenesis (Grivennikov et al., 2009), we analyzed the expression of the STAT3 target gene *birc5*, also known as *survivin*. The expression of *birc5* was down-regulated in $Apc^{Min/+}$::$ADAM17^{ex/ex}$ mice, whereas *sox-9* and *Il-6r* mRNA was more highly expressed in $Apc^{Min/+}$::$ADAM17^{ex/ex}$ mice. In addition, *yap-1*, *ctgf*, and *cyr61* mRNAs were lower in tissue from $Apc^{Min/+}$::$ADAM17^{ex/ex}$ mice compared with $Apc^{Min/+}$ mice (Fig. 6 B).

To obtain a more comprehensive view of transcriptome alterations that were associated with a lack of ADAM17, we performed RNA sequencing (RNA-seq) from nontumor and tumor tissue isolated from $Apc^{Min/+}$ and $Apc^{Min/+}$::$ADAM17^{ex/ex}$ mice. 3196 genes were up-regulated and 2883 genes were down-regulated in tumors of $Apc^{Min/+}$ mice versus $Apc^{Min/+}ADAM17^{ex/ex}$ mice. In nontumor intestinal tissue, 90 genes were up-regulated and 58 genes were down-regulated in $Apc^{Min/+}$ mice versus $Apc^{Min/+}$::$ADAM17^{ex/ex}$ mice. Principal component analysis showed only a partial separation of tumor and normal tissue by genotype (Fig. 7 A). The top 100 genes that were differentially expressed in $Apc^{Min/+}$ and $Apc^{Min/+}$::$ADAM17^{ex/ex}$ mice are depicted in Fig. 7 B, demonstrating a distinct gene expression signature in both mouse strains. The cluster of transcripts up-regulated in the $Apc^{Min/+}$ tumors contained several transcripts that have been previously related to CRC (e.g., T [brachyury], IL11, GATA4, JAG2; Hellebrekers et al., 2009; Kilic et al., 2011; Calon et al., 2012; Vaish et al., 2017). A STRING-based network analysis of the top 500 regulated transcripts confirmed this observation and showed densely connected subnetworks up-regulated in the $Apc^{Min/+}$ versus $Apc^{Min/+}$::$ADAM17^{ex/ex}$ tumors around Wnt signaling and cytokine/chemokine signaling (not depicted). Thus we analyzed conserved transcription factor binding sites

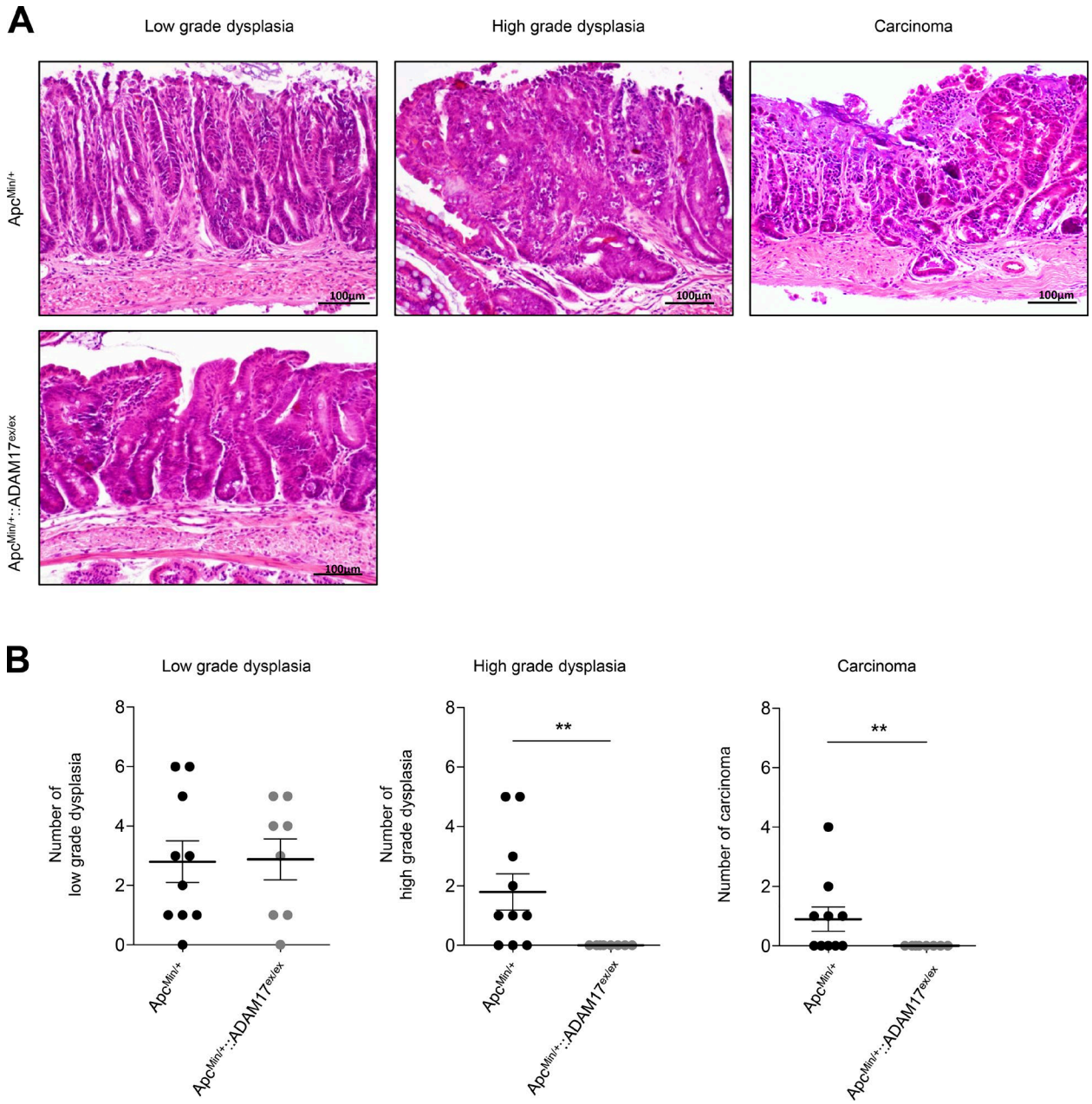

Figure 4. **Staging of dysplasias in Apc$^{Min/+}$ and Apc$^{Min/+}$::ADAM17$^{ex/ex}$ mice. (A)** Representative images of H&E-stained tissue of Apc$^{Min/+}$ mice and Apc$^{Min/+}$::ADAM17$^{ex/ex}$ mice. **(B)** Staging of dysplasia from Apc$^{Min/+}$ mice and Apc$^{Min/+}$::ADAM17$^{ex/ex}$ mice. Numbers of low-grade dysplasias, high-grade dysplasias, and carcinomas from Apc$^{Min/+}$ (n = 10) and Apc$^{Min/+}$::ADAM17$^{ex/ex}$ (n = 8) mice at 6 mo. **, P < 0.01 by Mann–Whitney test. Error bars indicate means ± SD.

(TFBSs) using the oPossum tool (Kwon et al., 2012) to identify enriched motifs using the full set of regulated transcripts. The analysis indicated an overrepresentation of genes regulated by transcription factors such as KLF4, SP1, and Zfx, which have been associated with cellular proliferation and stemness in Apc$^{Min/+}$ tumors, which is down-regulated in the absence of ADAM17 (Fig. 7 C). Most interestingly, in tumor tissue, TCFCP2L1, a known Wnt target (Qiu et al., 2015), and STAT3 TFBSs were enriched with high statistical scores (z-score and Fisher score). We next tested for known Wnt and STAT3 target genes (https://web.stanford.edu/group/nusselab/cgi-bin/wnt/target_genes; Pickert et al., 2009) and found several of them significantly more highly expressed in Apc$^{Min/+}$ mice compared with Apc$^{Min/+}$::ADAM17$^{ex/ex}$ mice (Table 1), again indicating that the IL-6-gp130-STAT3 axis was involved in intestinal tumorigenesis. Higher expression of T (brachyury) and SAA1 in the intestine of Apc$^{Min/+}$ mice compared with Apc$^{Min/+}$::ADAM17$^{ex/ex}$ mice was confirmed by immunohistochemistry (IHC; not depicted). In contrast, expression of amphiregulin protein was higher in the intestine of Apc$^{Min/+}$::ADAM17$^{ex/ex}$ mice, presumably because of the absence of ADAM17 shedding activity (not depicted), as has already been demonstrated for the EGF-R ligand TGFα, which accumulated at the cell surface of intestinal epithelial cells in the absence of ADAM17 (Chalaris et al., 2010). A network analysis

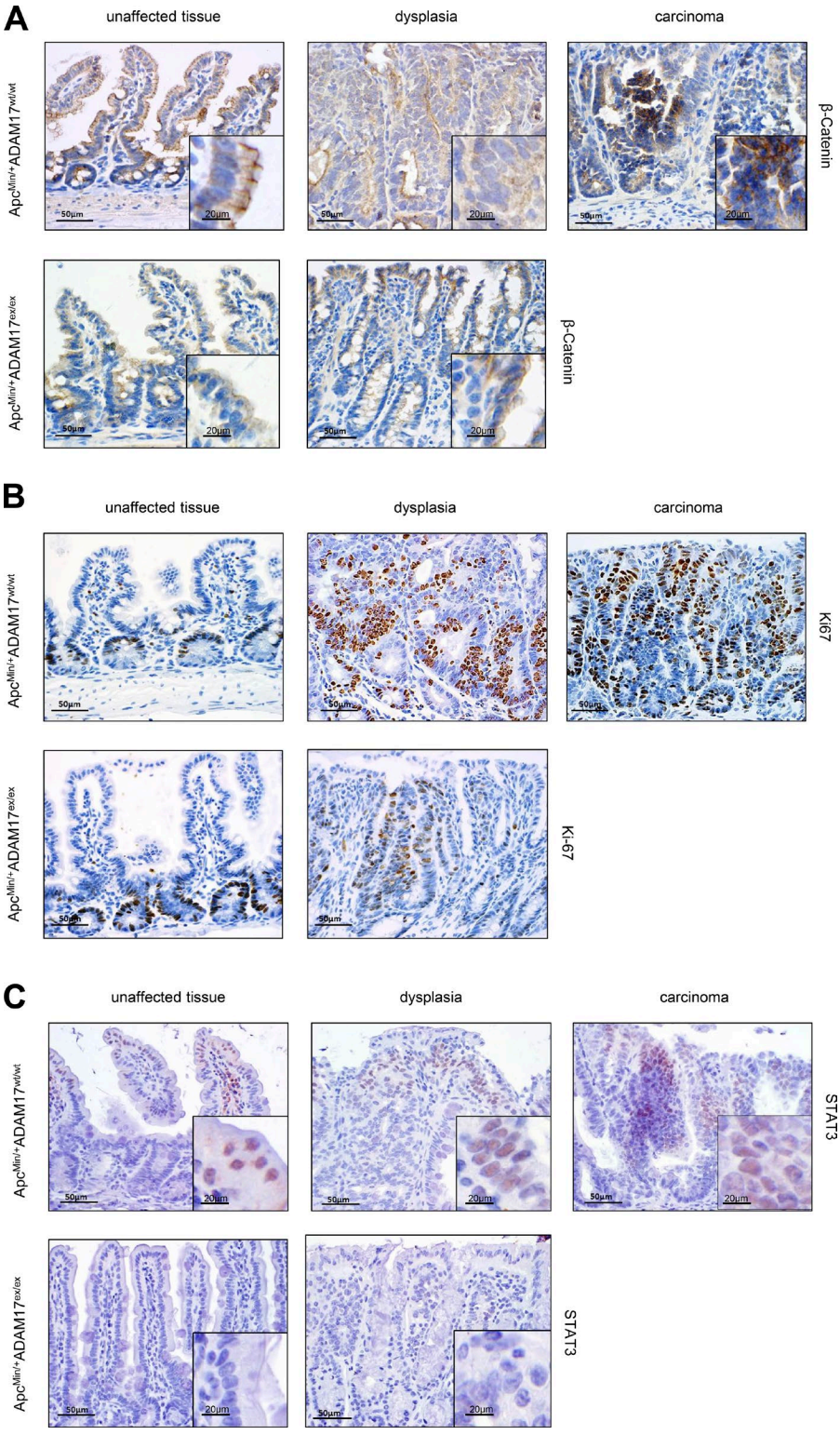

Figure 5. **Decreased β-catenin, Ki67, and nuclear STAT3 staining in $Apc^{Min/+}$::$ADAM17^{ex/ex}$ mice. (A–C)** Representative images of tissue from $Apc^{Min/+}$ mice and $Apc^{Min/+}$::$ADAM17^{ex/ex}$ mice stained for β-catenin (A), Ki-67 (B), and STAT3 (C). Small intestine from 24-wk-old $Apc^{Min/+}$ and $Apc^{Min/+}$::$ADAM17^{ex/ex}$ mice was used for IHC analysis to visualize β-catenin, Ki-67 and STAT3. $Apc^{Min/+}$ (n = 8) and $Apc^{Min/+}$::$ADAM17^{ex/ex}$ (n = 6) mice. Bars: (panels) 50 µm; (insets) 20 µm.

(based on STRING database) depicting the interaction matrix of up-regulated transcripts from unaffected tissue from $Apc^{Min/+}$ mice compared with $Apc^{Min/+}$::$ADAM17^{ex/ex}$ mice (corrected $P < 0.01$, no additional white nodes) revealed two larger modules around epithelial differentiation (e.g., keratins KRT7, 12 and 14, serpin B5, Muc5ac) and cell adhesion/cytoskeleton (e.g., integrin β6, laminin gamma 2 and β-actin). The network modules are depicted in Fig. 7 D.

Influence of ADAM17 on the intestinal microflora

The intestinal microbiome strongly affects barrier function and tumor formation (O'Keefe, 2016). Because ADAM17 is needed for proper intestinal barrier function (Chalaris et al., 2010), we wondered whether the absence of ADAM17 would have an influence on the composition of the intestinal microbiome. We profiled the fecal microbiome from unchallenged WT and $ADAM17^{ex/ex}$ mice

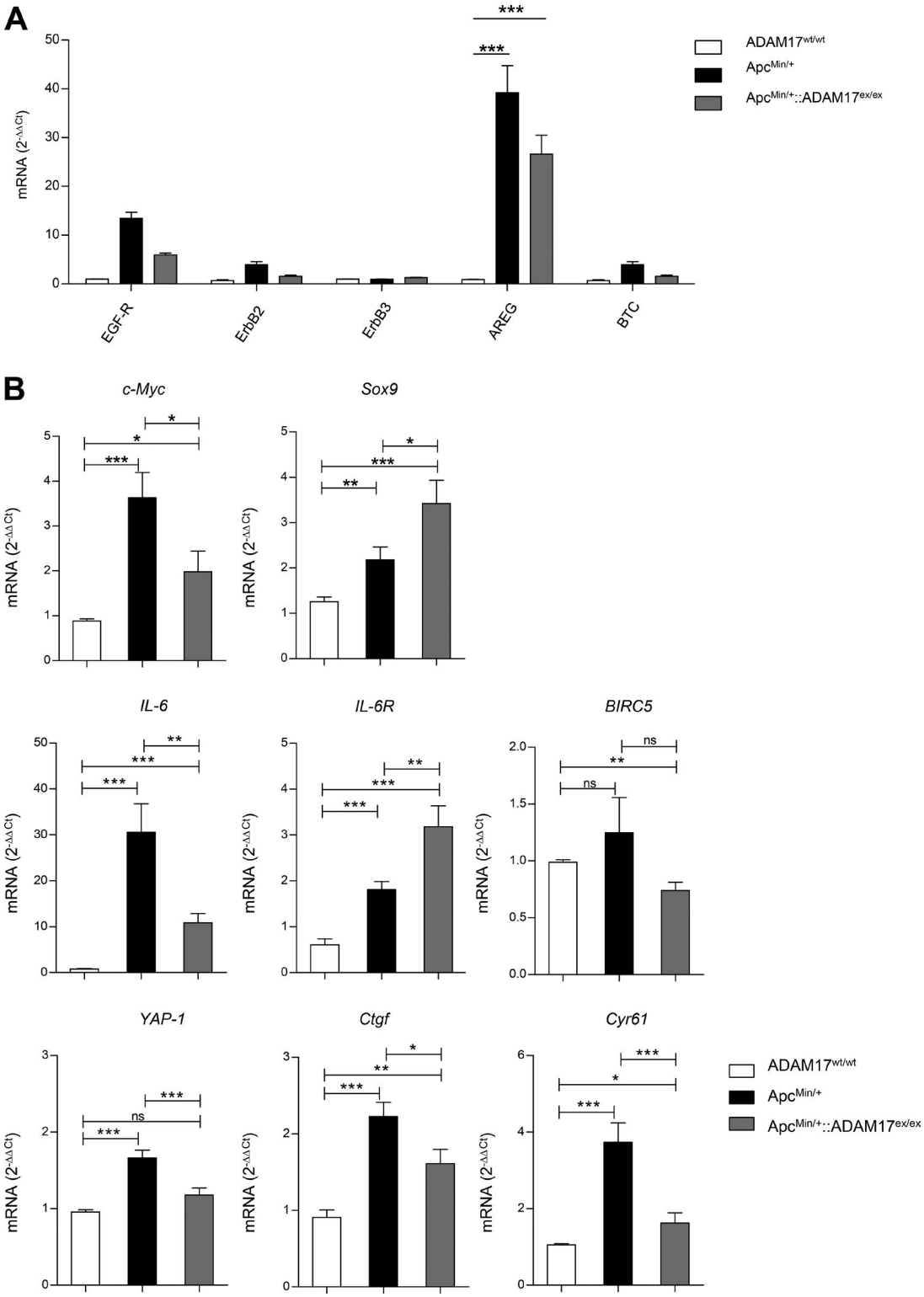

Figure 6. **Changes in gene expression in Apc$^{Min/+}$::ADAM17$^{ex/ex}$ mice. (A)** Laser microdissection and qRT-PCR analysis of ErbB family receptors and ligands from dysplasia of Apc$^{Min/+}$ mice and Apc$^{Min/+}$::ADAM17$^{ex/ex}$ mice. Tissue samples from six dysplasias from Apc$^{Min/+}$ mice (n = 3) and four dysplasias from Apc$^{Min/+}$::ADAM17$^{ex/ex}$ mice (n = 2) were collected via laser microdissection and compared with WT tissue. qRT-PCR analysis was performed in triplicate. ***, P < 0.001 by two-way ANOVA with Bonferroni post hoc test. **(B)** qRT-PCR analysis of selected target genes from Apc$^{Min/+}$ mice and Apc$^{Min/+}$::ADAM17$^{ex/ex}$ mouse tissue. 26 tumor samples obtained from Apc$^{Min/+}$ mice (n = 7) and 10 tumor samples obtained from Apc$^{Min/+}$::ADAM17$^{ex/ex}$ mice (n = 4) were compared with tissue samples from WT mice (n = 1). *, P < 0.05; **, P < 0.01; ***, P < 0.001; ns, nonsignificant by unpaired t test with Welch's correction. Error bars indicate means ± SD.

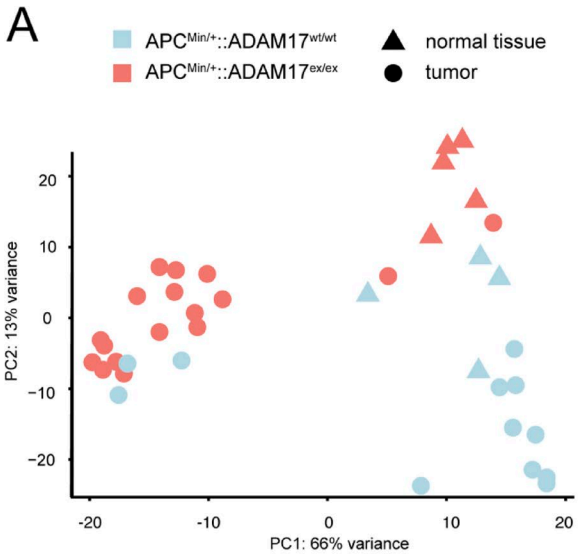

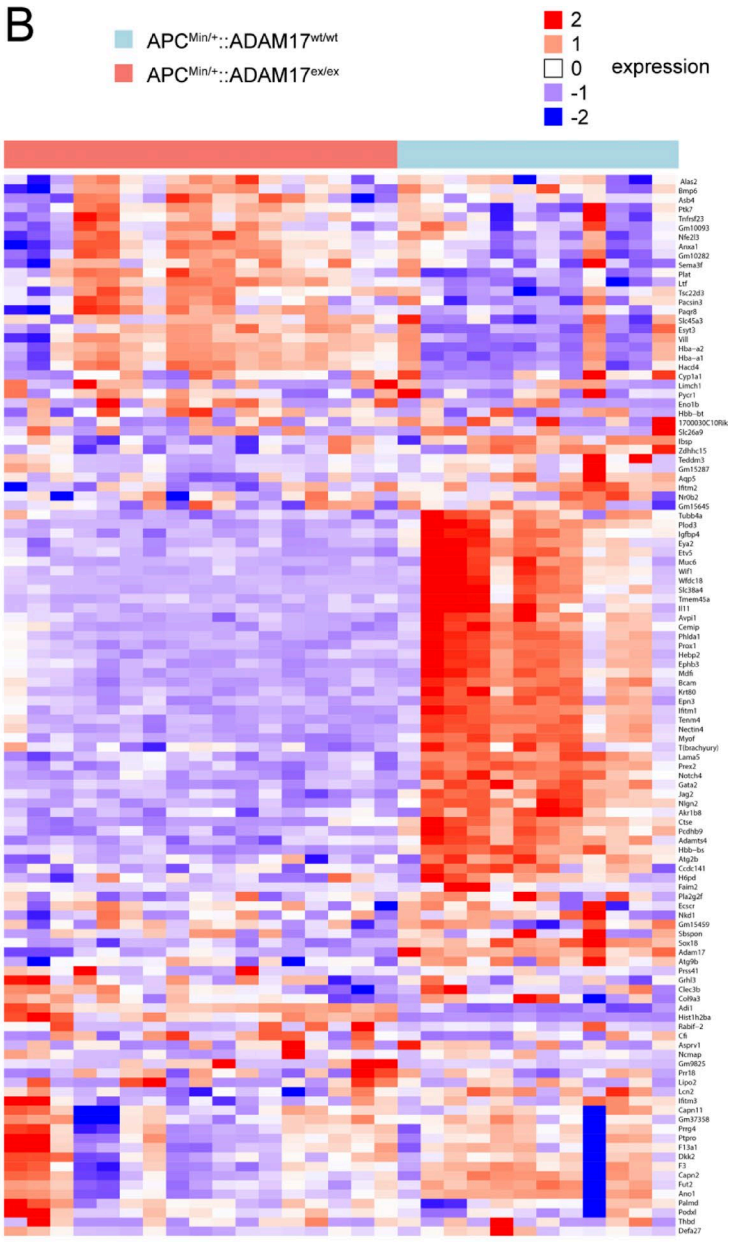

C

	TFBS	z-score	FS
tumor	KLF4	36.574	21.246
	Tcfcp2l1	30.341	13.909
	SP1	29.253	13.685
	MZF1	27.901	7.802
	EBF1	23.988	11.189
	ZNF354C	20.457	11.439
	MZF1	18.338	5.088
	Zfx	16.717	3.128
	Zfp423	15.807	5.215
	PPARG::RXRA	14.700	9.308
	INSM1	14.061	8.710
	ZEB1	13.481	11.434
	Hand1::Tcfe2a	11.706	5.568
	NHLH1	10.635	2.499
	ESR2	10.496	5.285
	NFE2L2	10.460	4.567
	Egr1	10.350	4.891
	Stat3	10.280	8.079
	NR4A2	10.035	4.851
	ELK1	9.415	5.666
healthy mucosa	KLF4	24.240	2.704
	SP1	17.985	1.094
	MZF1	17.981	1.388
	Tcfcp2l1	14.425	2.211
	MZF1	11.549	0.884
	ZEB1	10.631	2.359
	Stat3	10.411	1.522
	EBF1	9.684	1.610
	E2F1	9.566	1.359
	Zfx	9.505	0.481
	ZNF354C	9.389	3.326

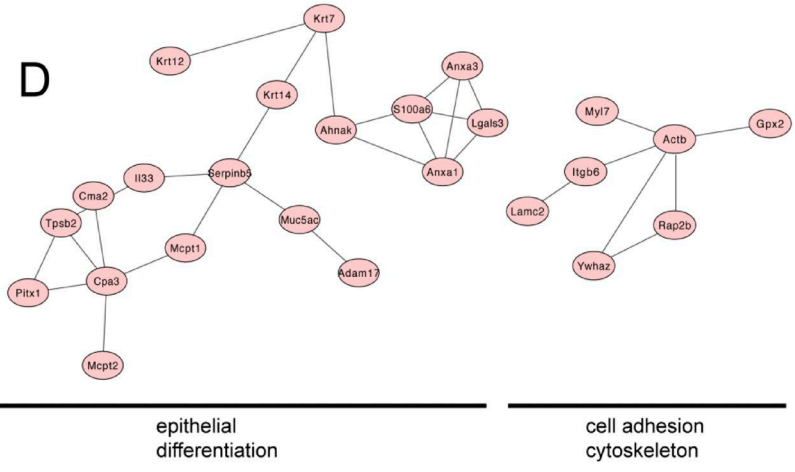

by analyzing the DNA sequence encoding the 16S rRNA. Multidimensional scaling revealed distinct clustering between WT, heterozygous ADAM17$^{wt/ex}$, and homozygous ADAM17$^{ex/ex}$ mice (Fig. S5 A). Significant changes were observed by operational taxonomical unit analysis of the respective genotypes depicted by heat map (Fig. S5 B). Interestingly, several bacterial taxa were depleted in the hypomorphic ADAM17$^{ex/ex}$ animals, which are involved in fermentation of dietary fiber into butyrate (*Coprococcus*, *Ruminococcus*; Fig. S5 B), a metabolic process protecting from colonic inflammation and carcinogenesis (Byndloss et al., 2017). Similar shifts in abundances have been detected in human CRC patients. Altogether, these data indicate that without any additional stimulus or pathological condition, the absence of ADAM17 has a remarkable effect on constitution of the intestinal microbiota, which might relate to the altered epithelial gene expression and contribute to tumorigenesis. Moreover, as shown in Fig. S5 C, inferred Kyoto Encyclopedia of Genes and Genomes (KEGG) categories in D-arginine, D-ornithine metabolism and inositol phosphate metabolism were significantly different between WT and ADAM17$^{ex/ex}$ mice. These metabolites are considered to be important for the maintenance of intestinal barrier function (Glover et al., 2016).

Tumor formation in the Apc$^{Min/+}$ model is dependent on IL-6 trans-signaling

EGF-R activity in myeloid cells is needed for tumorigenesis in the Apc$^{Min/+}$ model (Srivatsa et al., 2017) as well as in an inflammation-associated CRC model (Hardbower et al., 2017; Srivatsa et al., 2017). Because the sIL-6R is generated via limited proteolysis by the ADAM17 protease (Yan et al., 2016), and IL-6 expression in colonic myeloid CD11b-positive cells depends on the presence of the EGF-R (Srivatsa et al., 2017), we decided to analyze a possible role of the IL-6 trans-signaling pathway in tumorigenesis. This hypothesis was supported by our gene expression data, which showed that in Apc$^{Min/+}$ mice, Wnt and STAT3 regulated genes were significantly down-regulated in the absence of ADAM17 (Table 1). Furthermore, it has recently been shown that IL-6 is involved in the homeostasis of intestinal crypts (Aden et al., 2016; Jeffery et al., 2017) and that tumor formation in the Apc$^{Min/+}$ model was reduced on an IL-6$^{-/-}$ genetic background (Baltgalvis et al., 2008).

IL-6 trans-signaling can be specifically blocked by a soluble form of gp130 dimerized via a human IgG1 Fc (sgp130Fc) without affecting classic IL-6 signaling via the membrane-bound IL-6R (Jostock et al., 2001). We previously generated transgenic mice (sgp130Fc-tg mice) that expressed the sgp130Fc protein under the transcriptional control of a liver-specific promoter (Rabe et al., 2008). These mice were shown to be completely resistant to IL-6 trans-signaling–mediated pathologies (Lesina et al., 2011; Kraakman et al., 2015; Bergmann et al., 2017). We therefore compared tumor formation in Apc$^{Min/+}$, Apc$^{Min/+}$::IL-6$^{-/-}$, and Apc$^{Min/+}$::sgp130Fc-tg mice. There was no significant difference in the onset of tumor formation at 100 d (Fig. 8, A and B), as indicated by both tumor number and tumor size. However, as tumors progressed to 150 and 200 d, Apc$^{Min/+}$ mice on the IL-6$^{-/-}$ and sgp130Fc-tg genetic background showed similarly reduced tumor numbers and tumor areas. Although tumor numbers were initially lower in the absence of IL-6 classic and trans-signaling on the IL-6$^{-/-}$ genetic background (Fig. 8, C and D), after 200 and 300 d (Fig. 8, E–H), a time point when few Apc$^{Min/+}$ mice were still alive, Apc$^{Min/+}$::IL-6$^{-/-}$ and Apc$^{Min/+}$::sgp130Fc-tg mice showed strongly reduced tumor numbers and tumor sizes, indicating that IL-6 via the IL-6 trans-signaling pathway was involved in the later stages of Apc$^{Min/+}$ tumorigenesis. IHC analysis (Fig. 8 I) revealed a tendency to more intensive staining for pSTAT3 and pEGF-R in tumors compared with unaffected tissues. Tumors of Apc$^{Min/+}$ mice exhibited more pEGF-R reactivity than Apc$^{Min/+}$::IL-6$^{-/-}$ and Apc$^{Min/+}$::sgp130Fc-tg mice. In agreement with the experimental data shown in Fig. S4, there was no clear difference in infiltrating CD3-positive T cells (Fig. 8 I) and F4/80 macrophages (not depicted) in tumors of Apc$^{Min/+}$, Apc$^{Min/+}$::IL-6$^{-/-}$ and Apc$^{Min/+}$::sgp130Fc-tg mice. Collectively, our data indicate that tumor formation in the Apc$^{Min/+}$ model relies on IL-6 activity via the sIL-6R.

To extend a role for IL-6 trans-signaling to a preclinical setting that is more relevant for human CRC, we challenged WT mice with the alkylating mutagen azoxymethane (AOM). This treatment regimen replicated sporadic human CRC by reproducibly inducing tubular adenomas in the colon of mice in the absence of chronic inflammation conferred to by DSS or other mucosal irritants (Neufert et al., 2007). As shown in Fig. 9 A, we administered AOM to WT and sgp130Fc transgenic mice once a week for six consecutive weeks and analyzed tumor formation after 20 wk. The AOM treated sgp130Fc transgenic mice expressed sgp130Fc protein in the circulation (Rabe et al., 2008) at 2–6 µg/ml (not depicted). Tumors were visible upon endoscopy performed after 11 wk (Fig. 9 B). Protruding lesions visible upon endoscopy scored after 8, 11, and 17 wk

Figure 7. **RNA-seq analysis of tumors and unaffected tissue from Apc$^{Min/+}$ and Apc$^{Min/+}$::ADAM17$^{ex/ex}$ mice. (A)** Principal component analysis (PCA) of mRNA expression levels. The plot depicts the first two components, which explain the major part of the variation. Individual samples are color- and symbol-coded by tissue type (tumor and normal colonic tissue) and genotype (Apc$^{Min/+}$ vs. Apc$^{Min/+}$::ADAM17$^{ex/ex}$). We compared four nontumor tissue samples from Apc$^{Min/+}$ mice (n = 3) and six nontumor tissue from Apc$^{Min/+}$::ADAM17$^{ex/ex}$ mice (n = 3) with 12 tumor tissue samples from Apc$^{Min/+}$ mice (n = 3) and 17 tumor tissue samples from Apc$^{Min/+}$::ADAM17$^{ex/ex}$ mice (n = 4) as described in Materials and methods. **(B)** Hierarchical clustering of the top 100 (ranked by p-value) genes differentially expressed in tumor tissue from Apc$^{Min/+}$ versus Apc$^{Min/+}$::ADAM17$^{ex/ex}$ mice as described in Materials and methods. **(C)** Transcription factor binding inference using up-regulated gene sets from normal tissue and tumors. The table depicts enriched conserved TFBSs in the Apc$^{Min/+}$ tissue compared with Apc$^{Min/+}$::ADAM17$^{ex/ex}$ samples, using a fold change cutoff of >2-fold. Analysis was performed using the oPossum3 tool. z-score and Fisher test score (FS) represent two independent measures to determine the TFBS motifs that are overrepresented in the respective gene set against background. **(D)** STRING network depiction of transcripts up-regulated in unaffected Apc$^{Min/+}$::ADAM17$^{wt/wt}$ small intestinal tissue versus tissue derived from Apc$^{Min/+}$::ADAM17$^{ex/ex}$ mice. The network was constructed using default parameters without allowance of first-line interactors and/or additional white nodes.

Table 1. **Regulation of known Wnt and STAT3 target transcripts (RNA-seq)**

Target	Log2 fold change	Adjusted P-value	Increased in $Apc^{Min/+}$ normal mucosa
Wnt signature in $Apc^{Min/+}$ tumor tissue			
N-myc	1.2	8.51×10^{-6}	No
Axin2	1.1	7.13×10^{-5}	No
Mmp7	1.7	3.67×10^{-5}	No
Wnt5a	1.4	7.54×10^{-13}	No
Wnt7a	2.4	0.000181284	No
Efnb2	0.7	0.011594455	No
Efna2	0.9	0.012058086	No
Fgf18	1.8	0.00117603	No
Sox9	2.2	3.12×10^{-11}	No
Sox2	1.5	0.037838719	No
T	4.7	2.44×10^{-16}	No
Tbx1	2.8	4.02×10^{-10}	No
Tbx4	2.3	9.17×10^{-6}	No
Ccdn1	0.8	3.89×10^{-6}	No
Stat3 signature in $Apc^{Min/+}$ tumor tissue			
Reg3b	1.5	0.002154754	No
Reg4	1.7	0.000230609	No
Areg	1.9	5.16×10^{-7}	No
Lrg1	3.5	1.96×10^{-15}	No
Trf	1.3	0.000473624	No
Pla2g2f	3.5	1.58×10^{-14}	No
Fut9	1.6	0.022056147	No
Saa1	1.6	0.011289854	No
Saa3	2.8	4.88×10^{-12}	No
Socs3	0.6	2.05×10^{-6}	Yes
Ncald	0.8	0.005328861	No
Duox2	2.1	4.35×10^{-7}	No
Duoxa2	2.5	1.68×10^{-7}	Yes

revealed increasing numbers in WT mice, whereas significantly lower and nonincreasing numbers of lesions were found in sgp130Fc transgenic mice (Fig. 9 C). After 20 wk, the colons of WT mice exhibited several large tumors, whereas only a few small lesions were found in sgp130Fc transgenic mice (Fig. 9, D and E). Representative IHC stainings and quantifications of pSTAT3, pEGF-R, and CD3 are shown in Fig. 9 F. In agreement with the data from the $APC^{min/+}$ model shown in Fig. 8, there were no significant differences in pSTAT3, pEGF-R, and CD3 staining between the mice in the absence or presence of IL-6 signaling. These experiments revealed that sgp130Fc mice were extensively protected from AOM-induced intestinal tumor formation and therefore confirm and extend our findings obtained in the small intestine of a model for genetic susceptibility in familial adenomatous polyposis (i.e., $Apc^{Min/+}$ mice) to a model of colon tumorigenesis arising from the sporadic acquisition of driver mutations that underpins the majority of CRCs in humans.

Discussion

To date, treatment of CRCs with neutralizing EGF-R antibodies is hampered by the rapid development of resistance caused by mutations within the EGF-R signaling pathway and extrinsic and intrinsic resistance mechanisms. Here we show that in vitro and in vivo, EGF-R activation requires ADAM17 activity, which acts via shedding of membrane-bound EGF-R ligands. Furthermore, we show that tumorigenesis in the $Apc^{Min/+}$ model, which is known to require EGF-R activation (Roberts et al., 2002), is largely suppressed in the absence of ADAM17. Interestingly, this is not a result of reduced tumor progression, since the few tumors seen in $Apc^{Min/+}$::$ADAM17^{ex/ex}$ mice are of the same mean size as those seen in $Apc^{Min/+}$ control mice. Moreover, in the absence of ADAM17, the detected tumors were classified as low-grade dysplasias, whereas in the presence of ADAM17, high-grade dysplasias and carcinomas were also detected. Based on the recent finding that EGF-R on myeloid cells rather than on intestinal epithelial cells is required for tumor formation in the AOM/

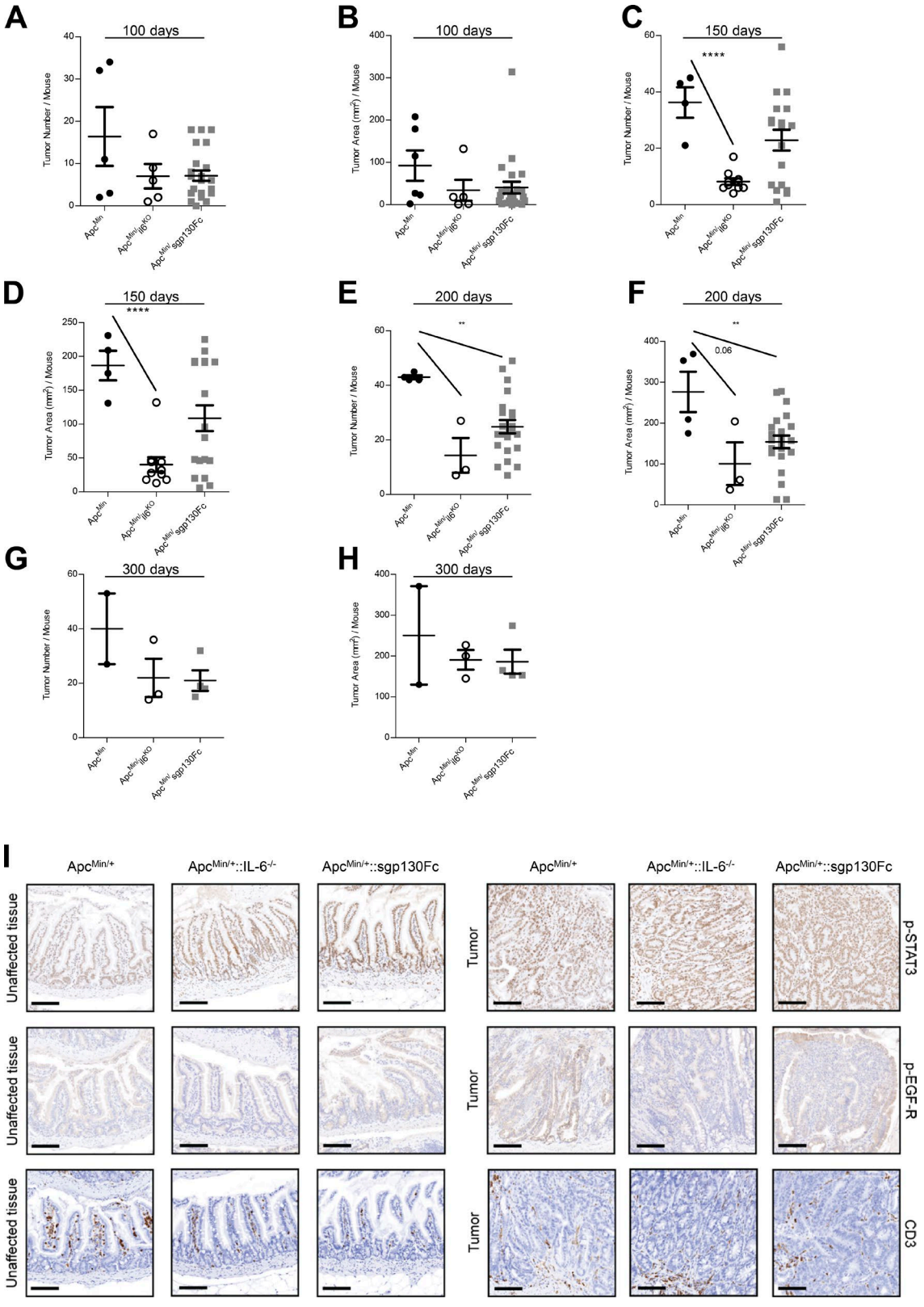

Figure 8. **Tumor number and tumor area of $Apc^{Min/+}$ mice depends on IL-6 trans-signaling via the sIL-6R. (A–H)** Tumor number (A, C, E, and G) and tumor area (B, D, F, and H) of $Apc^{Min/+}$ mice on WT, IL-$6^{-/-}$, and sgp130Fc transgenic background was determined after 100 d; $Apc^{Min/+}$, (n = 6); $Apc^{Min/+}$::IL-$6^{-/-}$, (n = 5); $Apc^{Min/+}$::sgp130Fc, (n = 23; A, B) 150 d; $Apc^{Min/+}$, (n = 4); $Apc^{Min/+}$::IL-$6^{-/-}$, (n = 10); $Apc^{Min/+}$::sgp130Fc, (n = 18; C, D), 200 d; $Apc^{Min/+}$, (n = 4); $Apc^{Min/+}$::IL-$6^{-/-}$, (n = 3); $Apc^{Min/+}$::sgp130Fc, (n = 22; E, F) and 300 d; $Apc^{Min/+}$, (n = 2); $Apc^{Min/+}$::IL-$6^{-/-}$, (n = 3); $Apc^{Min/+}$::sgp130Fc, (n = 4; G, H). Error bars indicate mean ± SEM. **(I)** Representative H&E images of tissue from $Apc^{Min/+}$, $Apc^{Min/+}$::IL-$6^{-/-}$ mice and $Apc^{Min/+}$::sgp130Fc mice at 150 d of age stained for pSTAT3, pEGF-R, and CD3. Bars, 100 µm. **, P < 0.01; ****, P < 0.0001.

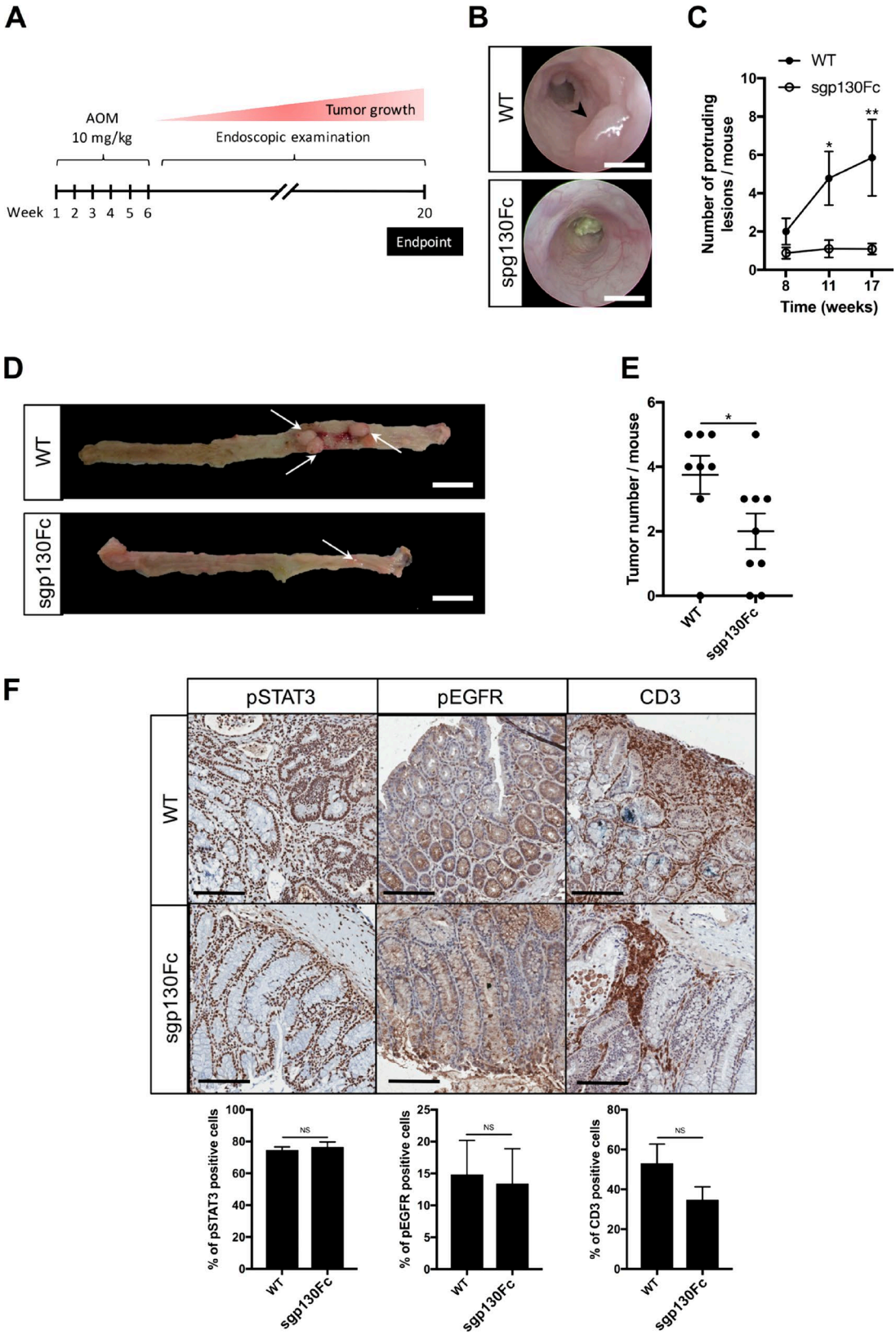

Figure 9. **Role of IL-6 trans-signaling in the sporadic AOM-induced tumor model. (A)** Schematic representation of the sporadic CRC model. WT or sgp130 transgenic mice were injected i.p. with AOM (10 mg/kg) once a week for a total of 6 wk. The spontaneous formation of distal colonic tumors was monitored by endoscopy once every week after 6 wk of AOM treatment. **(B)** Representative endoscopy images of distal colonic tumors (arrowhead) from WT or sgp130Fc transgenic mice at 11 wk. Bars, 2 mm at the plane of the head of the endoscope. **(C)** Representative number of protruding lesions from WT or sgp130Fc transgenic mice scored by endoscopy at 8, 11, and 17 wk. Data presented as mean ± SEM using $n \geq 6$ mice per cohort. *, $P < 0.05$; **, $P < 0.01$; by Student's *t* test.

DSS (Hardbower et al., 2017; Srivatsa et al., 2017) and $Apc^{Min/+}$ (Srivatsa et al., 2017) models, we demonstrate in two different intestinal tumor models a link between EGF-R, ADAM17, and IL-6, indicating that IL-6 trans-signaling is needed for efficient tumor formation in the intestine.

The $ADAM17^{ex/ex}$ mouse, with its massive reduction of ADAM17 protein levels in all tissues (Chalaris et al., 2010), has been used successfully to study the role of ADAM17 in various in vivo models including kidney fibrosis (Kefaloyianni et al., 2016), atherosclerosis (Nicolaou et al., 2017), and small vessel disease (Capone et al., 2016). With its residual ADAM17 activity, the $ADAM17^{ex/ex}$ mouse can serve as a model for the consequences of pharmacological inhibition of ADAM17, which will not lead to complete blockade of enzymatic activity. It has been shown that in $ADAM17^{ex/ex}$ mice, intestinal barrier function is compromised upon challenge (Chalaris et al., 2010). In the present study, we also demonstrate that, even without a challenge, the microbiome of $ADAM17^{ex/ex}$ mice is significantly changed compared with WT mice, indicating that by affecting the abundance of butyrate-producing bacterial taxa, ADAM17 may contribute to intestinal barrier function.

IL-6 plays a dual role in intestinal homeostasis. On the one hand, in the absence of IL-6, inflammation upon challenge with DSS is more severe because of compromised regeneration (Grivennikov et al., 2009). This is likely caused by reduced IL-6–stimulated STAT3 activation in response to the irritant (Grivennikov et al., 2009). Therefore, IL-6 is important for intestinal regeneration (Aden et al., 2016; Jeffery et al., 2017), and recombinant IL-6 improved colitis in a mouse model (Spehlmann et al., 2013; Srivatsa et al., 2017). On the other hand, IL-6 via IL-6 trans-signaling drives the inflammatory response in colitis, and sgp130Fc was sufficient to efficiently block inflammation in several colitis models (Atreya et al., 2000; Mitsuyama et al., 2006). Furthermore, it was shown in two different inflammation-associated colon cancer models that blockade of IL-6 trans-signaling resulted in significant inhibition of tumor growth (Becker et al., 2004; Matsumoto et al., 2010).

One important activity of ADAM17 is shedding of the IL-6R, which is a prerequisite of IL-6 trans-signaling (Riethmueller et al., 2017). It was surprising that blockade of IL-6 trans-signaling was sufficient for inhibition of tumor formation in the $Apc^{Min/+}$ model. IL-6 deficiency led to a decreased tumor load in this model (Baltgalvis et al., 2008), and we showed in the present study that IL-6 mRNA was massively up-regulated in $Apc^{Min/+}$ mice and down-regulated in the absence of ADAM17. Because blocking IL-6 trans-signaling was sufficient to strongly reduce tumor formation, these results now help to explain the unexpected observation that EGF-R on myeloid cells but not on intestinal epithelial cells was needed for tumor formation (Hardbower et al., 2017; Srivatsa et al., 2017). This notion is also supported by a recent study of mice with epithelial-specific ADAM17 deletion. In these mice, AOM treatment led only to a slight reduction of adenomas and cancer compared with the dramatic reduction in tumor incidence upon blockade of IL-6 trans-signaling (Mustafi et al., 2017). EGF-R stimulation on myeloid cells leads to IL-6 secretion (Srivatsa et al., 2017), and ADAM17 is needed for the cleavage of ligands of EGF-R such as amphiregulin. At the same time, ADAM17 is needed for shedding of the IL-6R from macrophages (Schumacher et al., 2015; Yan et al., 2016). Therefore, IL-6 induction and sIL-6R generation are both induced by ADAM17 activity, leading to stimulation of the intestinal epithelial cells via IL-6 trans-signaling.

Frequent somatic activating mutations in gp130 have been detected in inflammatory hepatocellular adenomas (Rebouissou et al., 2009). When such activated gp130 was expressed as a transgene in intestinal epithelial cells, proliferation and aberrant differentiation of these cells was observed, which depended on the activity of the transcriptional coactivator Yap (Taniguchi et al., 2015). When these transgenic mice were crossed with $Apc^{Min/+}$ mice, the animals developed very high tumor numbers in the jejunum and ileum. Tumor incidence was dramatically reduced in the absence of STAT3 and Yap, indicating that gp130 activation is crucial for tumor development in the $Apc^{Min/+}$ model (Taniguchi et al., 2017).

The important role of myeloid EGF-R activation in intestinal tumorigenesis, at least in mice, was unexpected (Hardbower et al., 2017; Srivatsa et al., 2017), although it was known that both M1 and M2 macrophages are activated by EGF-R stimulation (Hardbower et al., 2016). M1 macrophages are thought to be proinflammatory and antitumorigenic, whereas M2 macrophages are believed to act in a regenerative and protumorigenic fashion (Hardbower et al., 2016). Interestingly, differentiation of M2 macrophages requires IL-6 signaling via the membrane-bound IL-6R (Mauer et al., 2014), pointing to a plausible link between EGF-R and IL-6 in the intestine.

In patients with unresectable metastatic colon cancer, besides chemotherapy, EGF-R blockade by the neutralizing antibodies cetuximab and pantuximab is applied. In the investigated and analyzed patient cohorts of the present study, cetuximab was rarely administered, and then only in the context of combinatorial treatment protocols. Thus, statistical analyses of treatment response related to ADAM17 expression was renounced because of underpower and hardly objectifiable response rates according to the Response Evaluation Criteria in Solid Tumors (RECIST) after multisubstance treatments.

The majority of patients, which can account for up to 90%, show intrinsic resistance against anti–EGF-R antibodies as a result of KRAS mutations or mutations in other signaling pathways, such as BRAF or PIK3CA, which all lie downstream of the

(D) Photomicrographs of representative colons of mice of the indicated genotypes. Tumors are indicated by arrows. Bars, 1 cm. **(E)** Total tumor burden of WT or sgp130Fc transgenic mice at 20 wk. Data presented as mean ± SEM using $n \geq 8$ mice per cohort. *, $P < 0.05$ by Student's *t* test. **(F)** Representative IHC staining and quantification for pSTAT3, pEGFR, and CD3 from WT and sgp130Fc transgenic mice. Bars, 100 µm. Data presented as mean ± SEM and analyzed by Student's *t* test.

EGF-R (Van Emburgh et al., 2014). But even patients who respond to anti–EGF-R antibodies benefit from the treatment for only 3–12 mo because of acquired resistance mechanisms, which include mutations in the EGF-R precluding binding of cetuximab or amplification of the gene coding for the ErbB family member HER2 (Van Emburgh et al., 2014).

In this light, it is provocative that, although depending on EGF-R activity, colon cancer seems to require IL-6 trans-signaling. As we have shown, EGF-R stimulation of CD11b-positive colonic myeloid cells led to massive IL-6 induction (Srivatsa et al., 2017), and sIL-6R is generated by these cells (Tsukamoto et al., 2017). We showed in pancreatic cancer that IL-6 trans-signaling, in addition to oncogenic *KRAS*, is required for progression to ductal adenocarcinoma, and this progression was completely blocked in sgp130Fc transgenic mice (Lesina et al., 2011). The reduction in tumor load seen after blocking IL-6 signaling was less pronounced than the effect in ADAM17-deficient mice. Furthermore, it still needs to be determined whether a similar mechanism also operates in humans. Nevertheless, blocking IL-6 trans-signaling might be a new therapeutic strategy for the treatment of colon cancer that would not be affected by intrinsic or acquired resistance to EGF-R blockade.

Materials and methods

Mice

All mice were kept under barrier conditions in individually ventilated cages with species-appropriate husbandry in a 12-h light-dark cycle under standard conditions. All experiments involving mice were authorized by national law upon review of project proposals. C57BL/6J-Apc$^{Min/+}$/J mice were purchased from Jackson Laboratory (#002020) and were crossbred with IL-6$^{-/-}$, sgp130Fc transgenic mice or homozygous hypomorphic ADAM17$^{ex/ex}$ mice on a mixed C57BL/6::129 background. Generation of ADAM17 hypomorphic ADAM17$^{ex/ex}$ mice and sgp130Fc transgenic mice was previously described (Rabe et al., 2008; Chalaris et al., 2010).

Protein extraction

To extract proteins, cells were resuspended in ice-cold lysis buffer (50 mM Tris, 150 mM NaCl, 2 mM EDTA, 1% [vol/vol] NP-40, 1% [vol/vol] Triton X-100, and two complete-protease inhibitor cocktail tablets [Roche] per 50 ml). Animal tissues were mechanically disrupted by using the Precellys (Peqlab) homogenizer according to the supplier's instructions. The tissue was mixed with lysis buffer (50 mM Tris, 150 mM NaCl, 0.1% [vol/vol] SDS, 1% [vol/vol] Triton X-100, and 0.5% [wt/vol] sodium deoxycholate) and ceramic beads for homogenization. After homogenization, samples were incubated on ice for 60 min and centrifuged at 13,000 *g* for 15 min to collect the protein-containing supernatant. Protein concentrations were determined by BCA protein assay (Pierce; Thermo Fisher Scientific). To enrich glycosylated proteins, concanavalin A precipitation was performed. After incubation at 4°C overnight, the sample was centrifuged at 5,000 *g* and washed with ice-cold PBS.

Western blotting

Proteins in Laemmli buffer were boiled, centrifuged, and analyzed by discontinuous SDS-PAGE. Proteins were transferred onto PVDF membranes (Thermo Fisher Scientific) and blocked in 6% (wt/vol) dry nonfat milk. PVDF membranes were washed before adding the primary antibody and secondary antibody. Immunoreactive proteins were visualized by chemiluminescence.

Antibodies

Primary antibodies used for Western blot analysis were as follows: α-human ADAM17 (3976; Cell Signaling Technology); α-human EGF-R (4267; Cell Signaling Technology); and α-human pEGF-R (3777, Cell Signaling Technology). HRP-labeled secondary antibody for Western blot analysis was α-rabbit-IgG-POD (Dianova). Primary antibodies used for IHC were α-Ki-67 (12202, Cell Signaling Technology); α-β-catenin (610154, BD); α-human-STAT3 (sc-7179, Santa Cruz Biotechnology); α-p-STAT3 (sc-7993, Santa Cruz Biotechnology; 9145 Cell Signaling Technology); α-pEGF-R (GTX61353, 1:100; Genetex); and α-T (brachyury; AF2085; R&D Systems). Fluorochrome-conjugated secondary antibodies for IHC were α-rabbit-Cy3 (Dianova) and α-rabbit-FITC (Dianova).

Quantitative real-time PCR (qRT-PCR)

TRIzol reagent (Life Technologies; Thermo Fisher Scientific) was used to isolate RNA from animal tissue for cDNA synthesis and qRT-PCR according to the manufacturer's instructions. RNA from organoids was extracted using innuPREP RNA kit from Analytik Jena. RNA concentration and purity were spectrophotometrically analyzed by NanoDrop2000 (Thermo Fisher Scientific). For gene expression analysis, 1 µg RNA was reverse-transcribed by RevertAid H Minus Reverse transcription (Thermo Fisher Scientific). The cDNA was used as a template in a qRT-PCR assay on a LightCycler 480 system (Roche). All reagents were purchased from Roche. Primers were designed by using Roche Universal ProbeLibrary Assay Design Center. Primers and #UPL-Probes were as follows: mEGF-R_up_#10, 5′-TGTGCAAAGGAATTACGACCT-3′; mEGF-R_dn_#10, 5′-GTTGAGGGCAATGAGGACA-3′; mErbB2_up_#25, 5′-TTTGCCGGAGAGCTTTGAT-3′; mErbB2_dn_#25, 5′-TCTGGCCATGCTGAAATGTA-3′; mErbB3_up_#99, 5′-AAGTACAACCGGCCTCTGG-3′; mErbB3_dn_#99, 5′-CGACAAGACAAGCACTGACC-3′; mBTC_up_#68, 5′-CGGGTAGCAGTGTCAGCTC-3′; mBTC_dn_#68, 5′-ACAGTGGAGAATTGCAAGACC-3′; mAREG_up_#53, 5′-TCCAAGATTGCAGTAGTAGCTGTC-3′; mAREG_dn_#53, 5′-CCCTGAAGTATCGTTTCCAAAG-3′; mSox9_up_#25, 5′-CAGCAAGACTCTGGGCAAG-3′; mSox9_dn_#25, 5′-ATCGGGGTGGTCTTTCTTGT-3′; mIL-6_up_#6, 5′-GCTACCAAACTGGATATAATCAGGA-3′; mIL-6_dn_#6, 5′-CCAGGTAGCTATGGTACTCCAGAA-3′; mIL6R_dn_#53, 5′-ATCCTCTGGAACCCCACAC-3′; mIL6R_up_#53, 5′-GAACTTTCGTACTGATCCTCGTG-3′; mIL6ST_up_#85, 5′-AGGACCAAAGATGCCTCAAC-3′; mIL6ST_dn_#85, 5′-TGAAGGAAGTTCGAGGAGACA-3′; mYAP1_up_#99, 5′-TTCCGATCCCTTTCTTAACAGT-3′; mYAP1_dn_#99, 5′-GAGGGATGCTGTAGCTGCTC-3′; mCtgf_up_#85, 5′-CTGCAGACTGGAGAAGCAGA-3′; mCtgf_dn_#85, 5′-GCTTGGCGATTTTAGGTGTC-3′; mCyr61_up_#70, 5′-CGTCACCCTTCTCCACTTG-3′; mCyr61_dn_#70, 5′-CACTTGGGTGCCTCCAGA-3′; mBIRC5_up_#71, 5′-CCCGATGACAACCCGATA-3′; mBIRC5_dn_#71, 5′-CATCTGCTTCTTGACAGTGAGG-3′;

mcMyc_up_#77, 5′-CCTAGTGCTGCATGAGGAGA-3′; mcMyc_dn_#77, 5′-TCCACAGACACCACATCAATTT-3′; hEGF-R_#25_up, 5′-CAGAGTGATGTCTGGAGCTACG-3′; hEGF-R_#25_dn, 5′-GGGAGGCGTTCTCCTTTCT-3′; hErbB2_up_#16, 5′-GCCATGAGCAGTGTGCTG-3′; hErbB2_dn_#16, 5′-ACAGATGCCACTGTGGTTGA-3′; hErbB3_up_#25, 5′-CAATCCCCACACCAAGTATCA-3′; hErbB3_dn_#25, 5′-GATGTTTGATCCACCACAAAGTT-3′; hErbB4_up_#25, 5′-GCGAGACAAACCCAAACAAG-3′; hErbB4_dn_#25, 5′-CAATGCTTGAAGGTCTCCATT-3′; hBTC_up_#49, 5′-ACTGCATCAAAGGGAGATGC-3′; hBTC_dn_#49, 5′-TCTCACACCTTGCTCCAATG-3′; hEGF_up_#77, 5′-CGCAGGAAATGGGAATTCTA-3′; hEGF_dn_#77, 5′-CCATGATCACTGAGACACCAG-3′; hAREG_up_#38, 5′-CGGAGAATGCAAATATATAGAGCAC-3′; hAREG_dn_#38, 5′-CACCGAAATATTCTTGCTGACA-3′; hEREG_p_#13, 5′-AGGAGGATGGAGATGCTCTG-3′; hEREG_dn_#13, 5′-GAGGACTGCCTGTAGAAGATGG-3′; hTGFa_up_#38, 5′-CCCAGATTCCCACACTCAG-3′; hTGFa_up_#38, 5′-ACGTACCCAGAATGGCAGAC-3′; hNRG-2_up_#38, 5′-TGTGGTGGCCTACTGCAA-3′; hNRG-2_dn_#38, 5′-ACATGTTCTGCCGGAGGT-3′; hADAM17_up_#77, 5′-CGTTTTTCACAAAATTTCAAGGT-3′; hADAM17_dn_#77, 5′-CCCTAGAGTCAGGCTCACCA-3′; hADAM17_up_#53, 5′-GCCAGCAGAGAGATATATTAAAGACC-3′; and hADAM10_dn_#53, 5′-GGACCGTATTTATGGGGATAGTT-3′. Quantification of relative changes in gene expression pattern was determined with LightCycler 480 Software 1.5.0 (Roche Diagnostics). Relative mRNA levels were assessed by the $2^{-\Delta\Delta Ct}$ method. The ΔCt rates were calculated for each sample by normalization to the housekeeping gene GAPDH. Comparative real-time PCR results were performed in triplicate.

RNA-seq analysis

Tumor tissue and surrounding unaffected tissue of $Apc^{Min/+}$ and $Apc^{Min/+}$::$ADAM17^{ex/ex}$ mice were prepared fresh. To isolate total RNA from animal tissue for RNA-seq, the RNeasy Mini kit including a QIAshredder column (Qiagen) was used according to the supplier's instructions. RNA-seq was performed using standard protocols. Individual strand-specific sequencing libraries were prepared with the TruSeq stranded mRNA kit (Illumina) from 500 ng total RNA. Libraries were sequenced on an Illumina HiSeq2500 (125-nt paired-end reads) as described (Hasler et al., 2017). Reads were processed and mapped using the Bioconductor package DeSeq2 (Love et al., 2014). Network analyses were conducted using String database (Jensen et al., 2009) with default settings without allowing white nodes and additional interactors, and visualized in Cytoscape 3.5.1 (Shannon et al., 2003), and transcription factor binding site analyses were performed using the database oPossum 3.0 (Kwon et al., 2012). Data have been submitted to the Gene Expression Omnibus Repository: GEO submission GSE107759.

Microbiome analysis

Total DNA was isolated from fecal pellets using DNeasy PowerSoil kit (Qiagen). 16S ribosomal RNA gene variable region V3–V4 was amplified using bacterial domain–specific barcoded primer pair 319F and 806R as described (Hasler et al., 2017). Equal proportions of amplified amplicons from each sample were mixed and sequenced on the Miseq platform (Illumina). Sequences were quality controlled per the recommended Mothur MiSeq standard procedure (Kozich et al., 2013). Quality-controlled sequences were binned in phylotypes (Mothur-curated GreenGenes database) and operational taxonomical units (OTUs with 95% similarity). Alpha diversity indices were calculated on microbial profiles based on OTUs and genus-level phylotypes. Beta diversity analysis (nonmetric multidimensional scaling) was performed using unweighted uniFrac distances (10,000 iterations) in Mothur. Paired 16S rRNA gene reads (fastq) have been submitted to the European Nucleotide Archive (accession no. PRJEB23659).

Predicted functional analysis of microbiota

Predication of functional potential of microbial communities was performed by implementing PICRUSt (Langille et al., 2013). In brief, 16S rRNA gene sequences were mapped against the Mothur-curated GreenGenes reference database (gg_13_8_99). A rarefied shared phylotype file with equal numbers of sequences per sample was used to generate a biom file in Mothur. The resulting biom file was subjected to online PICRUSt galaxy terminal (http://huttenhower.sph.harvard.edu/galaxy/) to predict the metabolic potential. Phylotypes were first normalized for the predicated 16 S RNA gene copy number: KEGG pathway functions were predicted at level 3 with the use of KEGG Orthologues GreenGenes 13_5 database in PICRUSt. Predicted metagenomic profiles were analyzed in STAMP software (Parks and Beiko, 2010) to assess the significance of predicted functional differences in microbial communities in two groups. Statistical significance of differences was tested using White's nonparametric test with Benjamini–Hochberg false discovery rate correction.

ELISA

ELISA kits for mouse (DY989, R&D Systems) and human (DY262, R&D Systems) Amphiregulin were used according to the supplier's instructions.

Organoids

The isolated small intestine was opened longitudinally, washed with ice-cold PBS, and cut into small pieces (Sato et al., 2009). Tissue pieces were washed with ice-cold PBS and incubated in 2 mM EDTA and 0.5 mM DTT in PBS on ice for 30 min. After removal of the EDTA/DTT buffer, tissue pieces were resuspended in PBS, shaken vigorously, and allowed to settle for 5 min. The supernatant including released crypts was passed through a 100-µm cell strainer to remove cell debris and centrifuged at 500 *g*. The sedimented crypts were resuspended in Matrigel (Basement Membrane Matrix Growth Factor Reduced; Corning) at a 1:2 ratio with Gibco Advanced DMEM/F12 containing 1× GlutaMAX and 50 U/ml penicillin/streptomycin, plated in 24-well plates with 50 µl Matrigel GFR drops per well plus 500 µl individual medium, and cultured in a 37°C incubator at 5% CO_2 air content and 90% relative humidity. APC tumor medium for organoids from $Apc^{Min/+}$ and $Apc^{Min/+}$::$ADAM17^{ex/ex}$ mice contained 25 ng/ml Noggin (Peprotech), 40 ng/ml EGF (Peprotech), 1× B27 minus insulin (Gibco), 1× N2 (Gibco), 100 U/ml penicillin/streptomycin (Gibco), 1× GlutaMax (Gibco), 10 mM Hepes (Gibco), 1 mM *N*-acetyl-cysteine (Sigma-Aldrich), 50 µg/ml gentamycin (Gibco), and 50 µg/ml primocin (Invivogen) in Advanced DMEM/F12 medium (Gibco) and were added to the Matrigel. For passaging, the

Matrigel-embedded organoids were mechanically disrupted by resuspending in Advanced DMEM/F12 medium (Gibco) and passing through a needle (21G), centrifuged at 500 *g*, and resuspended in fresh Matrigel at a 1:2 ratio with Gibco Advanced DMEM/F12 containing 1× GlutaMax and 50 U/ml penicillin/streptomycin. The culture medium was changed every second day, and organoids were passaged twice a week at a 1:5 ratio. Organoids were seeded in 24-well plates, inhibitors were added as indicated in APC tumor medium, and organoids were incubated at 37°C for 72 h. For ELISA analysis, organoid supernatants were harvested, centrifuged at 1,000 *g* for 5 min, transferred into a new tube, and stored at −20°C until use. Each well was microscopically evaluated and photographed with the Nikon AZ100 microscope and NIS-Elements D 4.12.01 software to assess the number and size of every organoid.

Organoid IHC

For whole-mount immunofluorescent analysis, $APC^{min/+}$ and $APC^{min/+}$::$ADAM17^{ex/ex}$ intestinal organoids were grown in Matrigel spots in microclear CellStar 96-well plates (Greiner Bio One). Organoids were fixed with 3% PFA in PBS, permeabilized (PBS and 0.5% Triton X-100), quenched (PBS and 100 mM glycine), and blocked using serum-free protein block (X0909; Dako). Staining with primary antibodies was performed at 4°C overnight, followed by detection using AF488- or AF594-labeled secondary antibodies (Thermo Fisher Scientific). Images were acquired on an Olympus Fluoview 1000 confocal laser scanning microscope. The α-β-catenin antibody was used at 1:200, the α-Ki67 antibody at 1:200, the α-pEGF-R antibody at 1:100, the α-pSTAT3 antibody at 1:200, and the α-T (brachyury) antibody at 1:100.

Tissue microarrays

Tissue microarrays containing samples of 402 consecutive patients with UICC stage II–III CRC (Knösel et al., 2012) were cut and stained. In brief, tissue samples originated from patients who underwent surgery for colorectal carcinoma with negative margins in 1993–2006 at the surgical Department of the University Hospital of Friedrich-Schiller-University (Jena, Germany). Survival of patients was monitored until death or at least for 10 yr. The procedure concerning patients' data protection was according to regulations of the Friedrich-Schiller University (Jena, Germany). The ethical criteria in the tissue arrays used for this study are met by irreversible anonymization. The study protocol was in accordance with the ethical guidelines of the Helsinki Declaration.

Histology

Intestine was dissected and stored in ice-cold PBS. The junction between stomach and duodenum and the junction between ileum and cecum were cut to obtain the whole small intestine. The junction between cecum and colon was cut to obtain small intestine, which was repeatedly flushed with ice-cold PBS and opened longitudinally. For macroscopic assessment of tumor numbers and distribution, the intestine was photographed and evaluated with the NIS-Elements D 4.12.01 software. The intestine was rolled up with forceps from cranial to caudal part ("Swiss roll") and prepared for sectioning (Moolenbeek and Ruitenberg, 1981). For preparation of formalin-fixed paraffin-embedded (FFPE) tissue, the rolled tissue was fixed in 4% PFA overnight, washed in H_2O for 24 h, dehydrated by ascending alcohol series, and incubated in xylene for paraffin-embedded sections. Intestinal tissue was sectioned with a microtome at 4-µm thickness and stained in Azan or H&E after deparaffinization.

Histological stainings of FFPE tissue were performed by standard protocol before slides were covered with Eukitt. For antigen unmasking in the form of heat-induced epitope retrieval, protocols were used depending on primary antibody datasheet. If necessary, endogenous peroxidase activity was quenched by short incubation of FFPE tissue slides in 3% hydrogen peroxide. For permeabilization, slides were incubated with 0.1% (vol/vol) Triton X-100 in 1× PBS for 5 min. Specimens were blocked in 100 µl serum-free protein block (Dako; Agilent Technologies). Primary antibodies were diluted as recommended in antibody dilution solution (Invitrogen; Thermo Fisher Scientific) and incubated at 4°C overnight. After washing in PBS, the fluorochrome-conjugated secondary antibody was added in the dark. Sections were washed again in PBS in the dark before being mounted in ProLong Gold antifade reagent with DAPI (Thermo Fisher Scientific). If the protein of interest was targeted by an HRP-labeled secondary antibody, a DAB-substrate solution (0.05% DAB, 0.015% H_2O_2, and 0.01 M PBS, pH 7.2) was used to visualize labeled proteins. FFPE tissue slides were covered with DAB-substrate solution and incubated at RT. Slides were rinsed in ddH_2O, drained, and covered with mounting medium.

Tumor staging

Tumor staging was performed by two board-certified pathologists in a blinded manner according to described recommendations (Boivin et al., 2003). Infiltration of inflammatory cells in dysplasias was scored according to the following scheme: 0 = no infiltration of inflammatory cells, 1 = mild infiltration, 2 = moderate infiltration, and 3 = severe infiltration.

Cell culture

Human CRC cells were cultured in Iscove's modified Dulbecco's medium (IMEM), supplemented with 10% (vol/vol) FCS, 1% (vol/vol) sodium pyruvate, and 50 U/ml penicillin/streptomycin in a 37°C incubator at 5% CO_2 air content and 90% relative humidity. Adherent cells were washed with PBS, scraped off, and lysed in lysis buffer at 4°C for 4 h.

Laser microdissection

Mice were killed, and small intestines were removed and washed with ice-cold PBS. The small intestine was opened longitudinally, and Tissue-Tek O.C.T. compound was applied onto the tissue surface. The intestine was rolled into a Swiss roll and directly placed in a Tissue-Tek Cryomold (Sakura) with Tissue-Tek O.C.T. compound on dry ice in methylbutane until O.C.T. compound and tissue were completely frozen. Freshly prepared cryosections (12 µm) were placed on glass membrane slides and stained with Toluidine blue. A laser-coupled microscope was used to remove the tissue area of interest. The dissected tissue area was collected and directly lysed with a innuPREP RNA kit according to the manufacturer's instructions.

Statistics

Histological evaluation was done by using the Nikon AZ100 microscope and NIS-Elements D 4.12.01 software. Tumor staging was performed in a blinded fashion by board-certified pathologists. Significance was calculated by unpaired *t* test with Welch's correction test for the comparison of two means. Mann–Whitney *U* or Kruskal–Wallis tests were used to evaluate discontinuous observations. ANOVA was used to compare differences for multiple groups followed by Tukey's multiple comparison test or Bonferroni post hoc test. All tests were performed using GraphPad Prism 6 software. Statistical analyses of tissue microarray data were calculated with Fisher's exact test. The Kaplan–Meier method was used to calculate survival curves. Statistical differences in survival were assessed by log-rank test. For all analyses, statistical significance was defined as $P < 0.05$.

Online supplemental material

Fig. S1 shows EGF-R and ADAM17 expression data in colorectal carcinoma patients. Fig. S2 shows gene expression analysis of intestinal organoids from $Apc^{Min/+}$ and $Apc^{Min/+}$::$ADAM17^{ex/ex}$ mice. Fig. S3 shows the distribution of dysplasias in the intestine of $Apc^{Min/+}$ and $Apc^{Min/+}$::$ADAM17^{ex/ex}$ mice. Fig. S4 shows the infiltration of macrophages and T cells in the intestine of $Apc^{Min/+}$ and $Apc^{Min/+}$::$ADAM17^{ex/ex}$ mice. Fig. S5 depicts alterations in the intestinal microbiome upon loss of ADAM17.

Acknowledgments

We thank all members of the Rose-John laboratory for input. Dr. Athena Chalaris contributed to the concept at the initial phase of the study. We also thank Sabine Lagger (Vienna) for her help with immunohistochemistry.

This work was supported by the Deutsche Forschungsgemeinschaft, Bonn (CRC841, project C1 to D. Schmidt-Arras and S. Rose-John; CRC877, project A1 to S. Rose-John; SFB877, project A9 to C. Becker-Pauly; project A10 to C. Garbers; SFB877, project B9 to P. Rosenstiel; and the Cluster of Excellence "Inflammation at Interfaces"). The research of M. Sibilia was supported by Austrian Science Fund grant DK W1212 and the European Research Council Advanced Grant 694883.

S. Rose-John has acted as a consultant and speaker for AbbVie, Chugai, Genentech Roche, Pfizer, and Sanofi. He also declares that he is an inventor on patents owned by CONARIS Research Institute, which develops the sgp130Fc protein Olamkicept together with Ferring Pharmaceuticals and I-Mab. S. Rose-John has stock ownership in CONARIS. All other authors declare no competing financial interests.

Author contributions: Experiments were performed by S. Schmidt, N. Schumacher, J. Schwarz, M. Schlederer, M. Sibilia, M. Linder, J. Bolik, A. Rehman, A. Sinha, J. Lokau, A.-S. Cabron, F. Zunke, C. Becker-Pauly, P. Arnold, A. Preaudet, P. Nguyen, J. Huynh, S. Afshar-Sterle, A.L. Chand, J. Westermann, P.J. Dempsey, C. Garbers, D. Schmidt-Arras, P. Rosenstiel, T. Putoczki, and M. Ernst. Clinical samples were organized and data were analyzed by S. Tangermann, L. Kenner, A. Altendorf-Hofmann, T. Knösel, E.S. Gruber, and G. Oberhuber. S. Rose-John supervised experiments, analyzed data and wrote the manuscript. All authors analyzed the results and approved the final version of the manuscript.

Submitted: 13 September 2017
Revised: 22 December 2017
Accepted: 22 January 2018

References

Aden, K., A. Breuer, A. Rehman, H. Geese, F. Tran, J. Sommer, G.H. Waetzig, T.M. Reinheimer, S. Schreiber, S. Rose-John, et al. 2016. Classic IL-6R signalling is dispensable for intestinal epithelial proliferation and repair. *Oncogenesis.* 5:e270. https://doi.org/10.1038/oncsis.2016.71

Atreya, R., J. Mudter, S. Finotto, J. Müllberg, T. Jostock, S. Wirtz, M. Schütz, B. Bartsch, M. Holtmann, C. Becker, et al. 2000. Blockade of interleukin 6 trans signaling suppresses T-cell resistance against apoptosis in chronic intestinal inflammation: Evidence in Crohn disease and experimental colitis in vivo. *Nat. Med.* 6:583–588. https://doi.org/10.1038/75068

Avraham, R., and Y. Yarden. 2011. Feedback regulation of EGFR signalling: Decision making by early and delayed loops. *Nat. Rev. Mol. Cell Biol.* 12:104–117. https://doi.org/10.1038/nrm3048

Baltgalvis, K.A., F.G. Berger, M.M. Pena, J.M. Davis, S.J. Muga, and J.A. Carson. 2008. Interleukin-6 and cachexia in ApcMin/+ mice. *Am. J. Physiol. Regul. Integr. Comp. Physiol.* 294:R393–R401. https://doi.org/10.1152/ajpregu.00716.2007

Becker, C., M.C. Fantini, C. Schramm, H.A. Lehr, S. Wirtz, A. Nikolaev, J. Burg, S. Strand, R. Kiesslich, S. Huber, et al. 2004. TGF-beta suppresses tumor progression in colon cancer by inhibition of IL-6 trans-signaling. *Immunity.* 21:491–501. https://doi.org/10.1016/j.immuni.2004.07.020

Bergmann, J., M. Müller, N. Baumann, M. Reichert, C. Heneweer, J. Bolik, K. Lücke, S. Gruber, A. Carambia, S. Boretius, et al. 2017. IL-6 trans-signaling is essential for the development of hepatocellular carcinoma in mice. *Hepatology.* 65:89–103. https://doi.org/10.1002/hep.28874

Black, R.A., C.T. Rauch, C.J. Kozlosky, J.J. Peschon, J.L. Slack, M.F. Wolfson, B.J. Castner, K.L. Stocking, P. Reddy, S. Srinivasan, et al. 1997. A metalloproteinase disintegrin that releases tumour-necrosis factor-alpha from cells. *Nature.* 385:729–733. https://doi.org/10.1038/385729a0

Blobel, C.P. 2005. ADAMs: Key components in EGFR signalling and development. *Nat. Rev. Mol. Cell Biol.* 6:32–43. https://doi.org/10.1038/nrm1548

Boivin, G.P., K. Washington, K. Yang, J.M. Ward, T.P. Pretlow, R. Russell, D.G. Besselsen, V.L. Godfrey, T. Doetschman, W.F. Dove, et al. 2003. Pathology of mouse models of intestinal cancer: Consensus report and recommendations. *Gastroenterology.* 124:762–777. https://doi.org/10.1053/gast.2003.50094

Byndloss, M.X., E.E. Olsan, F. Rivera-Chávez, C.R. Tiffany, S.A. Cevallos, K.L. Lokken, T.P. Torres, A.J. Byndloss, F. Faber, Y. Gao, et al. 2017. Microbiota-activated PPAR-γ signaling inhibits dysbiotic Enterobacteriaceae expansion. *Science.* 357:570–575. https://doi.org/10.1126/science.aam9949

Calon, A., E. Espinet, S. Palomo-Ponce, D.V. Tauriello, M. Iglesias, M.V. Céspedes, M. Sevillano, C. Nadal, P. Jung, X.H. Zhang, et al. 2012. Dependency of colorectal cancer on a TGF-β-driven program in stromal cells for metastasis initiation. *Cancer Cell.* 22:571–584. https://doi.org/10.1016/j.ccr.2012.08.013

Capone, C., F. Dabertrand, C. Baron-Menguy, A. Chalaris, L. Ghezali, V. Domenga-Denier, S. Schmidt, C. Huneau, S. Rose-John, M.T. Nelson, and A. Joutel. 2016. Mechanistic insights into a TIMP3-sensitive pathway constitutively engaged in the regulation of cerebral hemodynamics. *eLife.* 5:e17536. https://doi.org/10.7554/eLife.17536

Chalaris, A., N. Adam, C. Sina, P. Rosenstiel, J. Lehmann-Koch, P. Schirmacher, D. Hartmann, J. Cichy, O. Gavrilova, S. Schreiber, et al. 2010. Critical role of the disintegrin metalloprotease ADAM17 for intestinal inflammation and regeneration in mice. *J. Exp. Med.* 207:1617–1624. https://doi.org/10.1084/jem.20092366

Egger, B., M.W. Büchler, J. Lakshmanan, P. Moore, and V.E. Eysselein. 2000. Mice harboring a defective epidermal growth factor receptor (waved-2) have an increased susceptibility to acute dextran sulfate-induced colitis. *Scand. J. Gastroenterol.* 35:1181–1187. https://doi.org/10.1080/003655200750056664

Glover, L.E., J.S. Lee, and S.P. Colgan. 2016. Oxygen metabolism and barrier regulation in the intestinal mucosa. *J. Clin. Invest.* 126:3680–3688. https://doi.org/10.1172/JCI84429

Grieve, A.G., H. Xu, U. Künzel, P. Bambrough, B. Sieber, and M. Freeman. 2017. Phosphorylation of iRhom2 at the plasma membrane controls mammalian TACE-dependent inflammatory and growth factor signalling. *eLife.* 6:e23968. https://doi.org/10.7554/eLife.23968

Grivennikov, S., E. Karin, J. Terzic, D. Mucida, G.-Y. Yu, S. Vallabhapurapu, J. Scheller, S. Rose-John, H. Cheroutre, L. Eckmann, and M. Karin. 2009. IL-6 and STAT3 signaling is required for survival of intestinal epithelial cells and colitis associated cancer. *Cancer Cell.* 15:103–113. https://doi.org/10.1016/j.ccr.2009.01.001

Haraldsdottir, S., and T. Bekaii-Saab. 2013. Integrating anti-EGFR therapies in metastatic colorectal cancer. *J. Gastrointest. Oncol.* 4:285–298.

Hardbower, D.M., K. Singh, M. Asim, T.G. Verriere, D. Olivares-Villagómez, D.P. Barry, M.M. Allaman, M.K. Washington, R.M. Peek Jr., M.B. Piazuelo, and K.T. Wilson. 2016. EGFR regulates macrophage activation and function in bacterial infection. *J. Clin. Invest.* 126:3296–3312. https://doi.org/10.1172/JCI83585

Hardbower, D.M., L.A. Coburn, M. Asim, K. Singh, J.C. Sierra, D.P. Barry, A.P. Gobert, M.B. Piazuelo, M.K. Washington, and K.T. Wilson. 2017. EGFR-mediated macrophage activation promotes colitis-associated tumorigenesis. *Oncogene.* 36:3807–3819. https://doi.org/10.1038/onc.2017.23

Hasler, R., R. Sheibani-Tezerji, A. Sinha, M. Barann, A. Rehman, D. Esser, K. Aden, C. Knecht, B. Brandt, S. Nikolaus, et al. 2017. Uncoupling of mucosal gene regulation, mRNA splicing and adherent microbiota signatures in inflammatory bowel disease. *Gut.* 66:2087–2097.

Hellebrekers, D.M., M.H. Lentjes, S.M. van den Bosch, V. Melotte, K.A. Wouters, K.L. Daenen, K.M. Smits, Y. Akiyama, Y. Yuasa, S. Sanduleanu, et al. 2009. GATA4 and GATA5 are potential tumor suppressors and biomarkers in colorectal cancer. *Clin. Cancer Res.* 15:3990–3997. https://doi.org/10.1158/1078-0432.CCR-09-0055

Hundhausen, C., D. Misztela, T.A. Berkhout, N. Broadway, P. Saftig, K. Reiss, D. Hartmann, F. Fahrenholz, R. Postina, V. Matthews, et al. 2003. The disintegrin-like metalloproteinase ADAM10 is involved in constitutive cleavage of CX3CL1 (fractalkine) and regulates CX3CL1-mediated cell-cell adhesion. *Blood.* 102:1186–1195. https://doi.org/10.1182/blood-2002-12-3775

Jeffery, V., A.J. Goldson, J.R. Dainty, M. Chieppa, and A. Sobolewski. 2017. IL-6 signaling regulates small intestinal crypt homeostasis. *J. Immunol.* 199:304–311. https://doi.org/10.4049/jimmunol.1600960

Jensen, L.J., M. Kuhn, M. Stark, S. Chaffron, C. Creevey, J. Muller, T. Doerks, P. Julien, A. Roth, M. Simonovic, et al. 2009. STRING 8--a global view on proteins and their functional interactions in 630 organisms. *Nucleic Acids Res.* 37(Database):D412–D416. https://doi.org/10.1093/nar/gkn760

Jones, S.A., J. Scheller, and S. Rose-John. 2011. Therapeutic strategies for the clinical blockade of IL-6/gp130 signaling. *J. Clin. Invest.* 121:3375–3383. https://doi.org/10.1172/JCI57158

Jostock, T., J. Müllberg, S. Ozbek, R. Atreya, G. Blinn, N. Voltz, M. Fischer, M.F. Neurath, and S. Rose-John. 2001. Soluble gp130 is the natural inhibitor of soluble interleukin-6 receptor transsignaling responses. *Eur. J. Biochem.* 268:160–167. https://doi.org/10.1046/j.1432-1327.2001.01867.x

Kefaloyianni, E., M.L. Muthu, J. Kaeppler, X. Sun, V. Sabbisetti, A. Chalaris, S. Rose-John, E. Wong, I. Sagi, S.S. Waikar, et al. 2016. ADAM17 substrate release in proximal tubule drives kidney fibrosis. *JCI Insight.* 1:e87023. https://doi.org/10.1172/jci.insight.87023

Kilic, N., S. Feldhaus, E. Kilic, P. Tennstedt, D. Wicklein, R. Wasielewski, C. Viebahn, H. Kreipe, and U. Schumacher. 2011. Brachyury expression predicts poor prognosis at early stages of colorectal cancer. *Eur. J. Cancer.* 47:1080–1085. https://doi.org/10.1016/j.ejca.2010.11.015

Kimelman, D., and W. Xu. 2006. beta-catenin destruction complex: Insights and questions from a structural perspective. *Oncogene.* 25:7482–7491. https://doi.org/10.1038/sj.onc.1210055

Kinzler, K.W., and B. Vogelstein. 1996. Lessons from hereditary colorectal cancer. *Cell.* 87:159–170. https://doi.org/10.1016/S0092-8674(00)81333-1

Knösel, T., Y. Chen, S. Hotovy, U. Settmacher, A. Altendorf-Hofmann, and I. Petersen. 2012. Loss of desmocollin 1-3 and homeobox genes *PITX1* and *CDX2* are associated with tumor progression and survival in colorectal carcinoma. *Int. J. Colorectal. Dis.* 27:1391–1399. https://doi.org/10.1007/s00384-012-1460-4

Kozich, J.J., S.L. Westcott, N.T. Baxter, S.K. Highlander, and P.D. Schloss. 2013. Development of a dual-index sequencing strategy and curation pipeline for analyzing amplicon sequence data on the MiSeq Illumina sequencing platform. *Appl. Environ. Microbiol.* 79:5112–5120. https://doi.org/10.1128/AEM.01043-13

Kraakman, M.J., H.L. Kammoun, T.L. Allen, V. Deswaerte, D.C. Henstridge, E. Estevez, V.B. Matthews, B. Neill, D.A. White, A.J. Murphy, et al. 2015. Blocking IL-6 trans-signaling prevents high-fat diet-induced adipose tissue macrophage recruitment but does not improve insulin resistance. *Cell Metab.* 21:403–416. https://doi.org/10.1016/j.cmet.2015.02.006

Kwon, A.T., D.J. Arenillas, R. Worsley Hunt, and W.W. Wasserman. 2012. oPOSSUM-3: Advanced analysis of regulatory motif over-representation across genes or ChIP-Seq datasets. *G3 (Bethesda).* 2:987–1002. https://doi.org/10.1534/g3.112.003202

Langille, M.G., J. Zaneveld, J.G. Caporaso, D. McDonald, D. Knights, J.A. Reyes, J.C. Clemente, D.E. Burkepile, R.L. Vega Thurber, R. Knight, et al. 2013. Predictive functional profiling of microbial communities using 16S rRNA marker gene sequences. *Nat. Biotechnol.* 31:814–821. https://doi.org/10.1038/nbt.2676

Lesina, M., M.U. Kurkowski, K. Ludes, S. Rose-John, M. Treiber, G. Klöppel, A. Yoshimura, W. Reindl, B. Sipos, S. Akira, et al. 2011. Stat3/Socs3 activation by IL-6 transsignaling promotes progression of pancreatic intraepithelial neoplasia and development of pancreatic cancer. *Cancer Cell.* 19:456–469. https://doi.org/10.1016/j.ccr.2011.03.009

Li, X., T. Maretzky, G. Weskamp, S. Monette, X. Qing, P.D. Issuree, H.C. Crawford, D.R. McIlwain, T.W. Mak, J.E. Salmon, and C.P. Blobel. 2015. iRhoms 1 and 2 are essential upstream regulators of ADAM17-dependent EGFR signaling. *Proc. Natl. Acad. Sci. USA.* 112:6080–6085. https://doi.org/10.1073/pnas.1505649112

Linardou, H., I.J. Dahabreh, D. Kanaloupiti, F. Siannis, D. Bafaloukos, P. Kosmidis, C.A. Papadimitriou, and S. Murray. 2008. Assessment of somatic k-RAS mutations as a mechanism associated with resistance to EGFR-targeted agents: A systematic review and meta-analysis of studies in advanced non-small-cell lung cancer and metastatic colorectal cancer. *Lancet Oncol.* 9:962–972. https://doi.org/10.1016/S1470-2045(08)70206-7

Love, M.I., W. Huber, and S. Anders. 2014. Moderated estimation of fold change and dispersion for RNA-seq data with DESeq2. *Genome Biol.* 15:550. https://doi.org/10.1186/s13059-014-0550-8

Matsumoto, S., T. Hara, K. Mitsuyama, M. Yamamoto, O. Tsuruta, M. Sata, J. Scheller, S. Rose-John, S. Kado, and T. Takada. 2010. Essential roles of IL-6 trans-signaling in colonic epithelial cells, induced by the IL-6/soluble-IL-6 receptor derived from lamina propria macrophages, on the development of colitis-associated premalignant cancer in a murine model. *J. Immunol.* 184:1543–1551. https://doi.org/10.4049/jimmunol.0801217

Mauer, J., B. Chaurasia, J. Goldau, M.C. Vogt, J. Ruud, K.D. Nguyen, S. Theurich, A.C. Hausen, J. Schmitz, H.S. Brönneke, et al. 2014. Signaling by IL-6 promotes alternative activation of macrophages to limit endotoxemia and obesity-associated resistance to insulin. *Nat. Immunol.* 15:423–430. https://doi.org/10.1038/ni.2865

McCart, A.E., N.K. Vickaryous, and A. Silver. 2008. Apc mice: Models, modifiers and mutants. *Pathol. Res. Pract.* 204:479–490. https://doi.org/10.1016/j.prp.2008.03.004

Mitsuyama, K., S. Matsumoto, S. Rose-John, A. Suzuki, T. Hara, N. Tomiyasu, K. Handa, O. Tsuruta, H. Funabashi, J. Scheller, et al. 2006. STAT3 activation via interleukin 6 trans-signalling contributes to ileitis in SAMP1/Yit mice. *Gut.* 55:1263–1269. https://doi.org/10.1136/gut.2005.079343

Moolenbeek, C., and E.J. Ruitenberg. 1981. The "Swiss roll": a simple technique for histological studies of the rodent intestine. *Lab. Anim.* 15:57–59. https://doi.org/10.1258/002367781780958577

Moss, M.L., S.L. Jin, M.E. Milla, D.M. Bickett, W. Burkhart, H.L. Carter, W.J. Chen, W.C. Clay, J.R. Didsbury, D. Hassler, et al. 1997. Cloning of a disintegrin metalloproteinase that processes precursor tumour-necrosis factor-alpha. *Nature.* 385:733–736. https://doi.org/10.1038/385733a0

Mustafi, R., U. Dougherty, D. Mustafi, F. Ayaloglu-Butun, M. Fletcher, S. Adhikari, F. Sadiq, K. Meckel, H.I. Haider, A. Khalil, et al. 2017. ADAM17 is a tumor promoter and therapeutic target in Western diet-associated colon cancer. *Clin. Cancer Res.* 23:549–561. https://doi.org/10.1158/1078-0432.CCR-15-3140

Neufert, C., C. Becker, and M.F. Neurath. 2007. An inducible mouse model of colon carcinogenesis for the analysis of sporadic and inflammation-driven tumor progression. *Nat. Protoc.* 2:1998–2004. https://doi.org/10.1038/nprot.2007.279

Nicolaou, A., Z. Zhao, B.H. Northoff, K. Sass, A. Herbst, A. Kohlmaier, A. Chalaris, C. Wolfrum, C. Weber, S. Steffens, et al. 2017. Adam17 deficiency

promotes atherosclerosis by enhanced TNFR2 signaling in mice. *Arterioscler. Thromb. Vasc. Biol.* 37:247–257. https://doi.org/10.1161/ATVBAHA.116.308682

O'Keefe, S.J. 2016. Diet, microorganisms and their metabolites, and colon cancer. *Nat. Rev. Gastroenterol. Hepatol.* 13:691–706. https://doi.org/10.1038/nrgastro.2016.165

Parks, D.H., and R.G. Beiko. 2010. Identifying biologically relevant differences between metagenomic communities. *Bioinformatics*. 26:715–721. https://doi.org/10.1093/bioinformatics/btq041

Peschon, J.J., J.L. Slack, P. Reddy, K.L. Stocking, S.W. Sunnarborg, D.C. Lee, W.E. Russell, B.J. Castner, R.S. Johnson, J.N. Fitzner, et al. 1998. An essential role for ectodomain shedding in mammalian development. *Science*. 282:1281–1284. https://doi.org/10.1126/science.282.5392.1281

Pickert, G., C. Neufert, M. Leppkes, Y. Zheng, N. Wittkopf, M. Warntjen, H.A. Lehr, S. Hirth, B. Weigmann, S. Wirtz, et al. 2009. STAT3 links IL-22 signaling in intestinal epithelial cells to mucosal wound healing. *J. Exp. Med.* 206:1465–1472. https://doi.org/10.1084/jem.20082683

Pietrantonio, F., C. Vernieri, G. Siravegna, A. Mennitto, R. Berenato, F. Perrone, A. Gloghini, E. Tamborini, S. Lonardi, F. Morano, et al. 2017. Heterogeneity of acquired resistance to anti-EGFR monoclonal antibodies in patients with metastatic colorectal cancer. *Clin. Cancer Res.* 23:2414–2422. https://doi.org/10.1158/1078-0432.CCR-16-1863

Prenzel, N., E. Zwick, H. Daub, M. Leserer, R. Abraham, C. Wallasch, and A. Ullrich. 1999. EGF receptor transactivation by G-protein-coupled receptors requires metalloproteinase cleavage of proHB-EGF. *Nature*. 402:884–888.

Qiu, D., S. Ye, B. Ruiz, X. Zhou, D. Liu, Q. Zhang, and Q.L. Ying. 2015. Klf2 and Tfcp2l1, two Wnt/β-Catenin targets, act synergistically to induce and maintain naive pluripotency. *Stem Cell Reports*. 5:314–322. https://doi.org/10.1016/j.stemcr.2015.07.014

Rabe, B., A. Chalaris, U. May, G.H. Waetzig, D. Seegert, A.S. Williams, S.A. Jones, S. Rose-John, and J. Scheller. 2008. Transgenic blockade of interleukin 6 transsignaling abrogates inflammation. *Blood*. 111:1021–1028. https://doi.org/10.1182/blood-2007-07-102137

Rebouissou, S., M. Amessou, G. Couchy, K. Poussin, S. Imbeaud, C. Pilati, T. Izard, C. Balabaud, P. Bioulac-Sage, and J. Zucman-Rossi. 2009. Frequent in-frame somatic deletions activate gp130 in inflammatory hepatocellular tumours. *Nature*. 457:200–204. https://doi.org/10.1038/nature07475

Riethmueller, S., P. Somasundaram, J.C. Ehlers, C.W. Hung, C.M. Flynn, J. Lokau, M. Agthe, S. Düsterhöft, Y. Zhu, J. Grötzinger, et al. 2017. Proteolytic origin of the soluble human IL-6R in vivo and a decisive role of N-glycosylation. *PLoS Biol.* 15:e2000080. https://doi.org/10.1371/journal.pbio.2000080

Roberts, R.B., L. Min, M.K. Washington, S.J. Olsen, S.H. Settle, R.J. Coffey, and D.W. Threadgill. 2002. Importance of epidermal growth factor receptor signaling in establishment of adenomas and maintenance of carcinomas during intestinal tumorigenesis. *Proc. Natl. Acad. Sci. USA*. 99:1521–1526. https://doi.org/10.1073/pnas.032678499

Rose-John, S., and P.C. Heinrich. 1994. Soluble receptors for cytokines and growth factors: Generation and biological function. *Biochem. J.* 300:281–290. https://doi.org/10.1042/bj3000281

Rose-John, S., K. Winthrop, and L. Calabrese. 2017. The role of IL-6 in host defence against infections: Immunobiology and clinical implications. *Nat. Rev. Rheumatol.* 13:399–409. https://doi.org/10.1038/nrrheum.2017.83

Sato, T., R.G. Vries, H.J. Snippert, M. van de Wetering, N. Barker, D.E. Stange, J.H. van Es, A. Abo, P. Kujala, P.J. Peters, and H. Clevers. 2009. Single Lgr5 stem cells build crypt-villus structures in vitro without a mesenchymal niche. *Nature*. 459:262–265. https://doi.org/10.1038/nature07935

Scheller, J., A. Chalaris, C. Garbers, and S. Rose-John. 2011a. ADAM17: A molecular switch to control inflammation and tissue regeneration. *Trends Immunol.* 32:380–387. https://doi.org/10.1016/j.it.2011.05.005

Scheller, J., A. Chalaris, D. Schmidt-Arras, and S. Rose-John. 2011b. The pro- and anti-inflammatory properties of the cytokine interleukin-6. *Biochim. Biophys. Acta*. 1813:878–888. https://doi.org/10.1016/j.bbamcr.2011.01.034

Schumacher, N., D. Meyer, A. Mauermann, J. von der Heyde, J. Wolf, J. Schwarz, K. Knittler, G. Murphy, M. Michalek, C. Garbers, et al. 2015. Shedding of endogenous interleukin-6 receptor (IL-6R) is governed by a disintegrin and metalloproteinase (ADAM) proteases while a full-length IL-6R isoform localizes to circulating microvesicles. *J. Biol. Chem.* 290:26059–26071. https://doi.org/10.1074/jbc.M115.649509

Shannon, P., A. Markiel, O. Ozier, N.S. Baliga, J.T. Wang, D. Ramage, N. Amin, B. Schwikowski, and T. Ideker. 2003. Cytoscape: a software environment for integrated models of biomolecular interaction networks. *Genome Res.* 13:2498–2504. https://doi.org/10.1101/gr.1239303

Sibilia, M., R. Kroismayr, B.M. Lichtenberger, A. Natarajan, M. Hecking, and M. Holcmann. 2007. The epidermal growth factor receptor: From development to tumorigenesis. *Differentiation*. 75:770–787. https://doi.org/10.1111/j.1432-0436.2007.00238.x

Siegel, R.L., K.D. Miller, and A. Jemal. 2016. Cancer statistics, 2016. *CA Cancer J. Clin.* 66:7–30. https://doi.org/10.3322/caac.21332

Sommer, A., F. Kordowski, J. Büch, T. Maretzky, A. Evers, J. Andrä, S. Düsterhöft, M. Michalek, I. Lorenzen, P. Somasundaram, et al. 2016. Phosphatidylserine exposure is required for ADAM17 sheddase function. *Nat. Commun.* 7:11523. https://doi.org/10.1038/ncomms11523

Spehlmann, M.E., C.F. Manthey, S.M. Dann, E. Hanson, S.S. Sandhu, L.Y. Liu, F.K. Abdelmalak, M.A. Diamanti, K. Retzlaff, J. Scheller, et al. 2013. Trp53 deficiency protects against acute intestinal inflammation. *J. Immunol.* 191:837–847. https://doi.org/10.4049/jimmunol.1201716

Srivatsa, S., M.C. Paul, C. Cardone, M. Holcmann, N. Amberg, P. Pathria, M.A. Diamanti, M. Linder, G. Timelthaler, H.P. Dienes, et al. 2017. EGFR in tumor-associated myeloid cells promotes development of colorectal cancer in mice and associates with outcomes of patients. *Gastroenterology*. 153:178–190. https://doi.org/10.1053/j.gastro.2017.03.053

Sternlicht, M.D., S.W. Sunnarborg, H. Kouros-Mehr, Y. Yu, D.C. Lee, and Z. Werb. 2005. Mammary ductal morphogenesis requires paracrine activation of stromal EGFR via ADAM17-dependent shedding of epithelial amphiregulin. *Development*. 132:3923–3933. https://doi.org/10.1242/dev.01966

Taniguchi, K., L.W. Wu, S.I. Grivennikov, P.R. de Jong, I. Lian, F.X. Yu, K. Wang, S.B. Ho, B.S. Boland, J.T. Chang, et al. 2015. A gp130-Src-YAP module links inflammation to epithelial regeneration. *Nature*. 519:57–62. https://doi.org/10.1038/nature14228

Taniguchi, K., T. Moroishi, P.R. de Jong, M. Krawczyk, B.M. Grebbin, H. Luo, R.H. Xu, N. Golob-Schwarzl, C. Schweiger, K. Wang, et al. 2017. YAP-IL-6ST autoregulatory loop activated on APC loss controls colonic tumorigenesis. *Proc. Natl. Acad. Sci. USA*. 114:1643–1648. https://doi.org/10.1073/pnas.1620290114

Terzic, J., S. Grivennikov, E. Karin, and M. Karin. 2010. Inflammation and colon cancer. *Gastroenterology*. 138:2101–2114. https://doi.org/10.1053/j.gastro.2010.01.058

Thul, P.J., L. Åkesson, M. Wiking, D. Mahdessian, A. Geladaki, H. Ait Blal, T. Alm, A. Asplund, L. Björk, L.M. Breckels, et al. 2017. A subcellular map of the human proteome. *Science*. 356:eaal3321. https://doi.org/10.1126/science.aal3321

Tobin, N.P., T. Foukakis, L. De Petris, and J. Bergh. 2015. The importance of molecular markers for diagnosis and selection of targeted treatments in patients with cancer. *J. Intern. Med.* 278:545–570. https://doi.org/10.1111/joim.12429

Tsukamoto, H., K. Fujieda, M. Hirayama, T. Ikeda, A. Yuno, K. Matsumura, D. Fukuma, K. Araki, H. Mizuta, H. Nakayama, et al. 2017. Soluble IL6R expressed by myeloid cells reduces tumor-specific Th1 differentiation and drives tumor progression. *Cancer Res.* 77:2279–2291. https://doi.org/10.1158/0008-5472.CAN-16-2446

Vaish, V., J. Kim, and M. Shim. 2017. Jagged-2 (JAG2) enhances tumorigenicity and chemoresistance of colorectal cancer cells. *Oncotarget*. 8:53262–53275. https://doi.org/10.18632/oncotarget.18391

Van Emburgh, B.O., A. Sartore-Bianchi, F. Di Nicolantonio, S. Siena, and A. Bardelli. 2014. Acquired resistance to EGFR-targeted therapies in colorectal cancer. *Mol. Oncol.* 8:1084–1094. https://doi.org/10.1016/j.molonc.2014.05.003

Yamada, Y., and H. Mori. 2007. Multistep carcinogenesis of the colon in Apc(Min/+) mouse. *Cancer Sci.* 98:6–10. https://doi.org/10.1111/j.1349-7006.2006.00348.x

Yan, I., J. Schwarz, K. Lücke, N. Schumacher, V. Schumacher, S. Schmidt, B. Rabe, P. Saftig, M. Donners, S. Rose-John, et al. 2016. ADAM17 controls IL-6 signaling by cleavage of the murine IL-6Rα from the cell surface of leukocytes during inflammatory responses. *J. Leukoc. Biol.* 99:749–760. https://doi.org/10.1189/jlb.3A0515-207R

Zhou, Y., and M.G. Brattain. 2005. Synergy of epidermal growth factor receptor kinase inhibitor AG1478 and ErbB2 kinase inhibitor AG879 in human colon carcinoma cells is associated with induction of apoptosis. *Cancer Res.* 65:5848–5856. https://doi.org/10.1158/0008-5472.CAN-04-3509